TÉCNICO LISBOA

Photovoltaic cells based on lead- and tin-perovskites

Ricardo Jorge T. M. Oliveira Carvalho

Thesis to obtain the Master of Science Degree in

Bioengineering and Nanosystems

Supervisor: Prof. Doctor Jorge Morgado

Examination Committee

Chairperson: Prof. Doctor Luís Fonseca

Supervisor: Prof. Doctor Jorge Morgado

Members of the committee: Prof. Doctor Ana Charas

May 2016

“Learn from yesterday, live for today, hope for tomorrow. The important thing is not to stop questioning”

Albert Einstein

“Memories of our lives, of our works and our deeds will continue in others”

Rosa Parks

Acknowledgments

First of all, I want to thank my supervisor, Prof. Jorge Morgado, for all the support and efforts provided during the realization of this thesis. Not only its help during practical work but also all the efforts to be present, comprehensive and to motivate me to not give up even when my thesis work went through some complicated moments.

Also, I want to address a special thank you to Ricardo Oliveira who spent lots of time clarifying some doubts and helping me during some occasional despair at the laboratory. Also, I want to thank all the laboratory colleagues for all the convenience and benefits that helped in different phases of my work and made the realization of this work easier.

An unconditional thank you to Mónica Araújo, Alexandre Ribeiro, Joana Farinhas, Cristiana Costa, Mónica Machado, Rajesh Veeravarapu and Luísa Mendonça for all the support and the sweet / funniest moments that often brighten my day.

I want to thank my parents for all the support that they provided me not only on this final step but also during all my academic journey.

Finally, I cannot forget all the friends with whom I lived and shared the best and worst moments. A huge special thanks to all of them.

Resumo

Vivemos numa sociedade cada vez mais industrializada e dependente de um numero crescente de recursos energéticos.

De entre as muitas alternativas energéticas ao nosso dispor, existe uma que se destaca pelo seu elevado potencial de aplicação: a energia solar. Esta fonte é o recurso energético mais abundante no mundo fornecendo aproximadamente 5,4 x 10^{26} J de energia por ano à Terra.

Tendo em conta a preocupação ambiental assente na produção de dispositivos fotovoltaicos, o principal foco desta tese é o desenvolvimento e produção de células solares de perovesquite com chumbo e estanho. Foi também testada a incorporação de PEO na solução de perovesquite numa tentativa de promover um aumento da eficiência (PCE).

Foram produzidas e testadas mais de uma centena de células fotovoltaicas com diferentes soluções de perovesquite e diferentes camadas aceitadoras / bloqueadoras de eletrões. Foram também testadas diferentes espessuras para as camadas de perovesquite por forma a melhorar o PCE.

Os resultados mais promissores surgem nas células solares de metil-amónio e iodeto de chumbo, com J_{sc} de 4,09 mA.cm^{-2}, V_{oc} de 0,57 V, FF de 37,82% e PCE de 0,88%.

Contudo, os resultados obtidos estão muito longe dos que se registam na literatura devido à extrema dificuldade em preparar filmes de perovesquite sem poros e de boa qualidade a partir de soluções. Apesar destes resultados um pouco dececionantes, é de realçar que este foi o primeiro trabalho na área das perovesquite no grupo de Eletrónica Orgânica do IT.

Palavras-chave: Perovesquite, células solares fotovoltaicas, metil-amónio, iodeto de estanho, iodeto de chumbo, cloreto de chumbo.

Abstract

We live in a society increasingly industrialized and progressively dependent on energy resources.

Among the many alternative energy sources at our disposal, there is one that stands out for its high application potential: the solar energy. This energy is the world's most abundant energy resource providing approximately 5.4 x 10^{26} J of energy per year on Earth.

Concerned about environmental issues related to the production processes of photovoltaic devices, the main focus of this thesis was to produce and develop perovskite based solar cells with tin and lead compounds. The incorporation of PEO on perovskite solution was also tested in an attempt to obtain higher power conversion efficiency (PCE) results.

More than one hundred cells were produced and tested with different perovskite solutions and different electron acceptor / blocking layers. Various perovskite thickness layers were investigated, trying to improve PCE.

The most promising result came from solar cells with methyl ammonium lead iodide, with a J_{sc} of 4.09 mA.cm^{-2}, V_{oc} of 0.57 V, FF of 37.82% and PCE of 0.88%.

However, the obtained results are far away from the literature ones due to the extremely difficulty to prepare pinhole-free and good quality perovskite films from solution. Despite these disappointing results, in terms of PCE, it should be mentioned that this has been the first project on perovskite solar cells in the Organic Electronics group at IT.

Keywords: Perovskite, photovoltaic solar cells, methyl-ammonium, tin iodide, lead iodide, lead chloride.

List of contents

List of Figures

List of Tables

Acronyms

AC	Alternate current
Bphen	Bathophenanthroline
CB	Conduction band
DC	Continuous current
DMF	Dimethylformamide
EAL	Electron acceptor layer
E_F	Fermi Energy
FF	Fill factor
FTO	Fluorine-tin oxide
HOMO	Highest occupied molecular orbital
HTM	Hole transporting material
J_{sc}	Short-circuit current density
LUMO	Lowest unoccupied molecular orbital
MAI	Methyl-ammonium iodine
OLED	Organic light-emitting diode
OPV	Organic photovoltaic cell
PCE	Power conversion efficiency
PEG	Polyethylene glycol
PEO	Polyethylene oxide
PVD	Physical vapor deposition
SCLC	Space charge-limited current
TCO	Transparent conductive oxide
VB	Valence band
V_{oc}	Open circuit voltage

1. Introduction

1.1. Motivation

Being a finalist of the Masters on Bioengineering and Nanosystems and having background in the energy conversion area, I found it very interesting to develop the master thesis project in a topic related with solar energy. The sun is an “endless” energy source that sustains life on Earth. A more direct use by man, implies the development of technology to harvest, convert and possibly store, that radiative energy. In view of the growing concerns about environmental changes, the technological challenges are related to developments avoiding or limiting the use of toxic materials. While the solar thermal systems are simple and efficient, huge efforts are being made to improve the photovoltaic systems, in view of the growing need of electrical power, not only to be used in combination with other power sources (such as wind and hydraulic) to supply the grid, but also to feed mobile devices and isolated houses. Reduction in costs (raw materials, fabrication, maintenance, replacement) and reduction of the environmental impact are the driving forces of the technology developments.

Based on the prospect of a more sustainable energy future it is important to study photovoltaic cells centered on relatively poorly known materials such as perovskites. Thus it would be possible to test not only existing perovskite systems but also to develop less toxic compositions. Centered on the idea of the relatively low cost involved in the preparation of perovskite solar cells, we also tried to use alternative materials such as tin in order to further reduce the toxic impact involved in the production of the photovoltaic devices.

The main goal of this thesis is to investigate different lead or tin perovskite compositions to be used in photovoltaic cells and to improve the actual performance. In particular, different devices were tested with alternative materials. The devices characterization involves current-voltage measurements, thickness analysis and UV/Vis absorption spectra. It is also important to denote that during this work I had the opportunity to probe different preparation and deposition techniques and also different surface treatments.

It is extremely important to focus efforts in order to develop new and clean energy alternatives in order to face the actual and future environmental impacts that arise from the increasing need of energy.

1.2. Socio-economic environment

We live in a society increasingly industrialized and globalized which focuses its efforts on growing technological empowerment [1]. This approach makes us increasingly dependent on energy resources. For instance, it is known that, only in 2012, a total of 21.474 toe (tons of oil equivalent) of primary energy was consumed in Portugal, from which, 16.158 toe represent the consumption from non-renewable

energy sources like coal, oil and natural gas. The remaining 4.477 toe represent the contribution of renewable energy [2]. Given these data, it is important to bear in mind the need for increasingly sustainable energy sources that can support the future energy requirements.

Among the many alternative energy sources at our disposal, there is one that stands out for its high application potential: the solar energy. The sun is the world's most abundant energy resource providing approximately 5.4 x 10^{26} J of energy per year on Earth [3]. This photonic energy can be used to generate heat (solar thermal systems), solar fuels (such as hydrogen) or to generate, directly, electric energy, via the use of photovoltaic cells. These systems can capture energy from the sun (photons) and convert it into electrical energy.

The growing usage of these energetic systems began in the 1980s. The most traditional applications were initially confined to campers and boats, temporary power needs for some disaster situations or for remote communication stations repeaters. In 1990s, the photovoltaic (PV) energy began to be widely used as an energy source for urban centers, private homes and office buildings becoming extremely important for the development of the modern world [4]. Today, ever more, this technology is used in order to satisfy the growing energy needs. Solar cells are widely used not only on Earth but also in Space applications (e.g. in satellites or robots).

1.3. Main applications and evolution

Since the discovery of the photovoltaic phenomenon, efforts were focused on developing a wide variety of technologies in order to promote sustainable solutions for crucial human needs, not only on our planet but also in outer space.

Solar electric energy main applications on Earth are [4]:

- Remote stand-alone without/with battery storage
- Residential grid connected with DC to AC inverter
- Photovoltaic fields (solar farms) for utility power generation

One of the most fundamental applications in the past was on water pumping, avoiding the use of battery cells. This system was very valuable for crop irrigation or clean water supply for remote villages without energy networks [4]. Today, there is an exponential growth in the number of homes on the electrical network that are using photovoltaic systems to produce electricity in order to save on costs of peak electric power.

The users can sell the excess electricity they generate to other users that are connected in the grid, balancing the primary costs of the usually large investment.

The fundamental step in this area was the discovery of the photovoltaic effect by Edmond Becquerel and its explanation by Albert Einstein [5].

Many efforts have been made over the years to convert sun light into electric energy. The first material that was tested in these systems was selenium, although this attempt failed because this material could not provide enough energy to power electrical equipment. Yet, this work proved that a solid material could convert light into electricity without heat or moving parts [5].

Another breakthrough in this field was the discovery of a method to grow silicon single-crystals in 1918 by a Polish scientist, Jan Czochralski [5]. The doors for a new energy Era were opened, without precedents.

In 1954, the first photovoltaic system created used silicon as semiconductor. Initially, the power output was very low (about 4% efficiency) [5]. Today, with the many advances that have been made, the efficiency of these solar cells has reached a pleasant value of 21.5% [6]. However, there is a high cost of production for these types of solar cells, especially when they use crystalline silicon structures. The production cost in 1977 was 76.67 $/watt (US dollars) and in 2013 it abruptly decreased to 0.36 $/watt, but it is still high to compete with the other offers on the energy market [7]. This is currently the biggest obstacle to promote solar energy as viable main energy source.

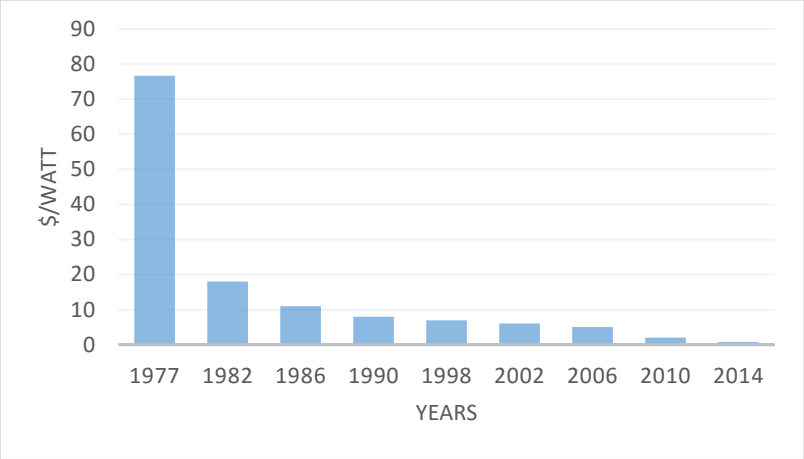

Figure 1.3-1. Evolution of silicon solar cells cost [7]

1.4. Photovoltaic technology

The three most viable photovoltaic technology systems, from the commercially point of view, are [8]:

- Thin films
- Thick silicon film
- Third generation technologies

Thin film technologies can be the cheapest option at a first point, because they require much less material. However, there are some critical issues when considering this technology, such as yield, reliability, manufacturing scale up and efficiency [8]. Nowadays, the most used semiconductor in this type of films is the amorphous-silicon (a-Si) which represents 64% of the thin film market [9]. Organic materials have the potential to become an important alternative avoiding some toxicity problems caused by other thin film technologies and reducing costs. However it is necessary to improve their stability and efficiency [10].

The thick film crystalline silicon layers are the most used in solar cells. They can be made from mono- or poly-crystalline silicon, which possesses a low absorption coefficient (the capacity of photon absorption at specific wavelengths). These layers need to be very thick (approximately 100 μm) to absorb a significant part on the incoming light. Nowadays, this technology is still expensive ($3.8/Watt in 2010) [11] for residential purposes but for large commercial systems this cost decreases by 42% [8].

The third generation technologies can be labeled as a “contrast of the thin film structures” because they have better efficiencies (better ability to excite bound electrons in the crystalline structure of a specific material) but at the same time they are yet quite expensive [8]. For example, quantum dots can generate a theoretical maximum efficiency of 42%, but an efficiency of only 2% has so far been reported [8]. It is essential to improve the equilibrium between the cost of production and the desired efficiency [12].

In order to overcome these price limitations, it is essential to look for new alternatives, with respect to cheaper materials to fabricate solar cells without compromising the already achieved efficiency.

1.5. Physical principles behind photovoltaic cells

The typical structure of photovoltaic cells is based on glass substrate, bottom electrode and hole transport material (HTM) to collect, the positive charges generated from the photoactive layer which is composed by a planar or blend donor-acceptor semiconductors. On top of the active layer is placed the electron acceptor layer (EAL) and the top electrode which collect the negative charges. The semiconductor materials that are present in these solar cells may belong to the organic or inorganic family of materials allowing the creation of singular or hybrid devices.

Every inorganic semiconductor has an energy diagram composed by a valence band (VB) and a conduction band (CB) separated by an energy gap. The valence band is where all the electrons are confined at 0K. Being this valence band completely occupied, there are no mobile charge carriers. Therefore, at 0K, all semiconductors are insulators. Only when the valence electrons are excited to the conduction band, they become mobile and can, therefore, carry electric current [13]. At the same time, for each electron that is excited to the conductive band, a hole (missing electron, to which we associate a positive charge) is created in valence band, which is also mobile. When an electric field is applied, both free holes (+) and free electrons (-) migrate towards opposite directions [14].

The excitation of electrons from the valence band (VB) to the conduction band (CB) is usually promoted by temperature. This explains the increase of the semiconductors electrical conductivity with temperature. Alternatively, this excitation can also be carried out by photon absorption. For this photoexcitation to occur it is necessary that the photon energy is equal to or higher than the semiconductor band gap [14].

The smaller the energy band gap, the lower the photon energy required to promote that excitation. Per each photon with sufficient energy that is absorbed, a free electron and a free hole can be generated. After this excitation, we may separate and collect the free charges if we apply an electric field. Alternatively, the electron may return to the valence band, by recombining with the hole (electron-hole recombination). The energy associated to this return of the electron to the CB can be re-emitted, a process named luminescence, or can be converted into heat. These are the basic processes that occur in semiconductors following light absorption, making them the required photoactive materials in photovoltaic applications [14].

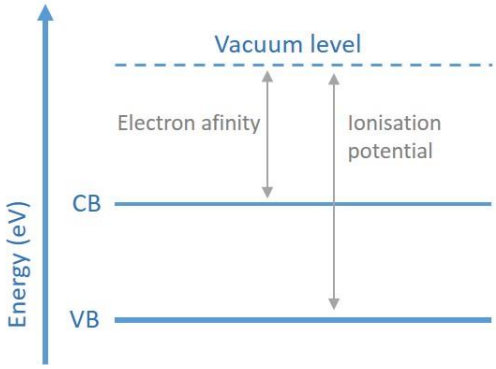

Figure 1.5-1. Energy band diagram of an inorganic semiconductor. CB corresponds to the bottom of the conduction band and CV is the top of the valence band

Semiconductors are the key component of solar cells. The photoactive layer is able to absorb the photons generating free charges (electric energy). In order to separate the free electron charges (-) from the hole charges (+) solar cells make use of a p-n junction. We thereby create an organized movement of charges upon photon absorption. When the cell is short-circuited, it generates the maximum current, named short-circuit current (J_{sc}). When in open circuit, it generates a voltage, named open circuit voltage (V_{oc}), which correspond to the maximum energy of the charge carriers (this is equivalent to the electromotive force of a battery).

Organic semiconductors, which can be for instance conjugated polymers, possess intrinsic physical properties that are somehow similar to inorganic ones. Each organic semiconductor has an energy gap between occupied bonding π orbitals, being HOMO the highest occupied molecular orbital and empty anti-bonding π (or π*) orbitals, being the LUMO the lowest unoccupied molecular. These semiconductors have charge defects (polarons) which are associated to non-degenerating ground states. Polarons can have positive or negative charges.

Instead of a p-n junction, organic photovoltaic cells combine two different materials in the active layer, one acting as excited state electron donor and the other acting as acceptor. When a photon with equal or higher energy of the semiconductor gap is absorbed by the active layer (usually the donor material) it will excite an electron from a π to a π* orbital, creating pair of positive and negative polarons. This pair has significant binding energy, acting as a single entity (quasi-particle) named exciton.

The photo-generated excitons will diffuse to the interface between the two different semiconductors (donor/acceptor heterojunction) where they can be dissociated if the energy difference between the LUMO of donor and the LUMO of acceptor is favorable, typically ca. 0.5 eV. After the dissociation process, negative charges move in the acceptor semiconductor and positive charges move in the donor semiconductor.

Finally, positive charges are collected at the highest work function electrode and negative charges are collected at the electrode with lower work function. This organized current is promoted by the internal electric field which is created by the asymmetric electrodes. In order to improve charge collection, hole-transporting layers (HTL) may be inserted between the highest work function electrode and the active layer and electron-transporting layers (ETL) may be inserted between the lowest work function electrode and the active layer.

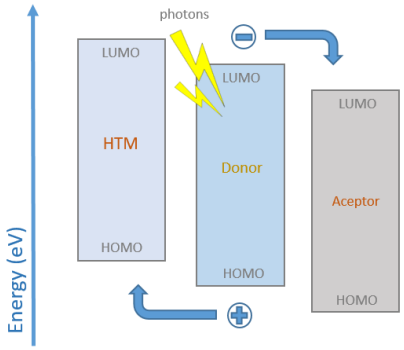

Figure 1.5-2. Energy diagram representing the flux of positive and negative charges

1.6. Equivalent circuit of solar cells

In ideal solar cells, the photo generated current density, J_{sc}, is provided by a DC current source stimulated under light illumination. Figure 1.6-1 shows the equivalent circuit of an ideal photovoltaic device.

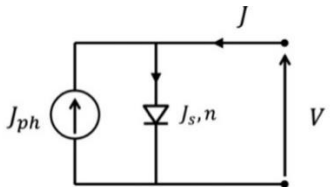

Figure 1.6-1. Equivalent circuit for an ideal solar cell [15]

In figure 1.6-1 J_{ph} represents the photo generated current density, J_s the current density of the diode, J is the current flow in an external load and V the applied voltage. When a controlled voltage is applied to a diode, the current flows in the circuit promoting a “rectangular” J-V curve with almost 100% of FF.

In real cases, parasitic resistances cannot be avoidable leading to energy losses and promoting poor performance efficiency and a much smaller FF [15]. Figure 1.6-2 shows the equivalent circuit of a practical solar cell with a series and shunt resistances to simulate equivalent energy losses. R_{sh} represents the shunt resistance and R_s the series resistance.

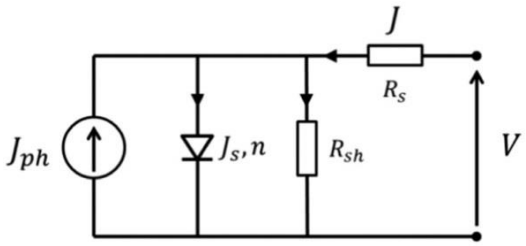

Figure 1.6-2. Equivalent circuit for real solar cells [15]

1.7. Organic and inorganic hetero-junctions

A hetero-junction is a connection between two different conductive, semi conductive or non-conductive materials where their interface is continuous between them [16]. With a hetero-junction it is possible to create a depletion region near the interface between two different materials where both charge carriers (+) and (-) lose their mobility [17]. When the photons are absorbed by these charges they become excited and acquire mobility again. After electron excitation, the charges move to opposite directions according to the nature of each doped semiconductor [18]. The positive charge carriers move to p-type semiconductor and the negative charge carriers move to n-type semiconductor. Applying a voltage to this p-n junction promotes a continuous flow of charge carriers to each electrode respectively. It is also important to notice that the interface state density at the surfaces should be minimal in order to minimize the recombination of charges [18]. When a semiconductor shows a superior number of electrons it is called n-type, on the other hand, when a semiconductor shows a superior number of holes it is called p-type [14].

The hetero-junctions that are mainly used in solar cells are the doped semiconductor-semiconductor junction. They can be classified in isotype (n-n) or anisotype (p-n) [14]. The one that is mostly used in inorganic solar cells is the p-n junction.

In figure 1.7-1 it is possible to observe the main differences present at the junction interface between inorganic and organic semiconductors. While in the inorganic semiconductors the p-n

heterojuntions are continuous at the interface between them, in the organic semiconductors the interface between donnor-aceptor is interrupted with an energy offset between both HOMO and LUMO levels.

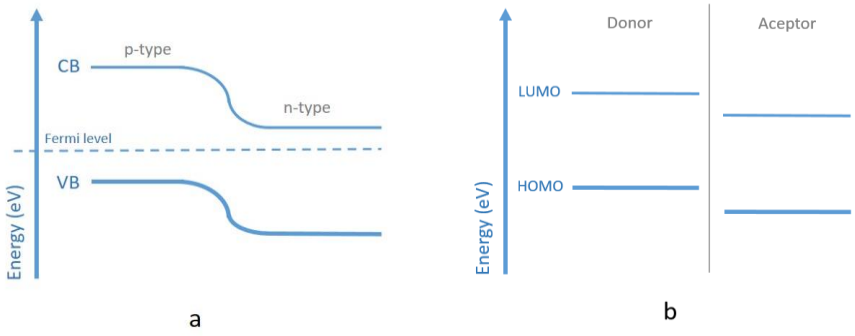

Figure 1.7-1. Junction diagram for inorganic a) and organic b) semiconductors

Due to the internal electric field promoted by hetero-junction, the opposite charges are separated for each one of the two semiconductors creating an ordered movement of charges between the two contacts [6].

1.8. Perovskites

Since 2009, a new material type, perovskite, is being investigated as a candidate to replace the well-known silicon as light harvester on solar cells [3]. This material is much less expensive than silicon, can be processed from solution and nowadays it can offer an efficiency that rivals that of the crystalline silicon-based devices.

Perovskite is the name of a mineral, calcium titanium oxide ($CaTiO_3$), found by Gustav Rose in 1839 in the Ural Mountains of Russia. Its name is dedicated to the Russian mineralogist L.A. Perovsk. Currently, the term perovskite is not only used for this mineral but also for all ABX_3, where X can be oxygen, carbon, nitrogen or halogen, A represents the larger cation that occupies octahedral cube-area coordinated by twelve X anions; and B is the smaller cation, which is stabilized in the octahedral region and coordinated by six X anions [19] (see Figure 1.8-1).

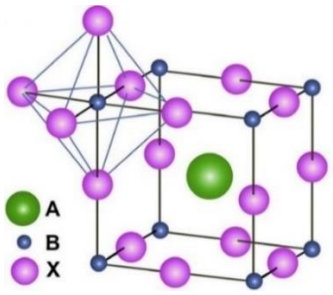

Figure 1.8-1. Crystalline structure of perovskite [19]

The most studied perovskites are the oxides due to their electrical properties such as superconductivity. However, at present, there is another very interesting type of perovskites, called halide perovskites. Layered organometallic halide perovskites are one of the most studied perovskite materials because they show a semiconductor-to-metal transition [20]. They offer the possibility to obtain a semiconducting material with low band gap facilitating electronic transitions between VB and CB [19].

Perovskites that contain halide anions allow monovalent or divalent cations on A and B sites to achieve charge neutrality. In the case of $CH_3NH_3PbX_3$ perovskites, the cation present in the A site is $CH_3NH_3^+$ and the cation present in the B site is Pb_2^+. Figure 1.8-2 shows the unit cell of cubic $CH_3NH_3PbI_3$ perovskite that was used in the preparation of the solar cell samples with the lead atom in the center of that cubic structure coordinated by six iodines.

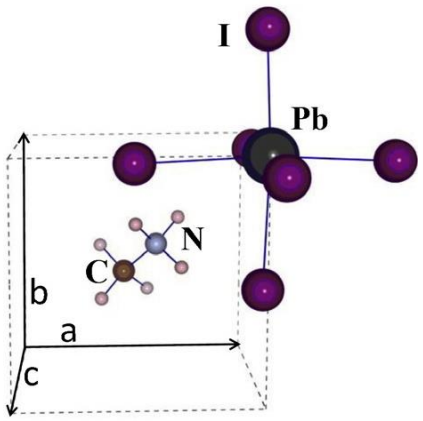

Figure 1.8-2. Unit cell of cubic CH3NH3PbI3 perovskite [19]

2. Evolution of lead- and tin-perovskite solar cells

2.1. Lead-perovskite solar cells

Solar cells based on lead halide perovskites, ($CH_3NH_3PbX_3$, X = Cl, Br, I), have been obtained an increasing interest in the last five years. Their PCE has been steadily growing increasing, from approximately 3.8% to more than 19% in just 4 years approaching the remarkable value of the silicon based solar cells [21]. The major improvements were focused on the materials used in the different layers and the thickness and nature of the hole-transporting material (HTM) layers.

2.1.1. First inorganic sensitized perovskite solar cell

In 2009, Miyasaka et al. [22] reported the first dye-sensitized solar cells based on $CH_3NH_3PbX_3$ (X = Br, I) perovskites.

Miyasaka et al. prepared two different solar cells named a) and b) with different perovskite solutions. The first had $CH_3NH_3PbBr_3$ and the second had $CH_3NH_3PbI_3$, deposited as nano-crystalline particles self-organized on a TiO_2 layer, acting as n-type semiconductor. The PCE value of the first cell was 3.13% while for the second cell a value of 3.81% was obtained [22].

The structure of these solar cells is based on the dye-sensitized solar cells developed by O'Regan and Gratzel in 1991. In Gratzel's experiment, the hole conductor is a liquid electrolyte that allowed the reduction of the charge leakages and increased the power conversion efficiencies (PCE).

This structure is composed by a series of different layers as shown in figure 2.1.1-1 [19]:

1. Conducting F-doped SnO_2-coated glass (transparent conductive oxide)
2. Compact TiO_2 layer
3. Dye-sensitized hetero-junction (TiO_2/HTM)
4. Gold electrode

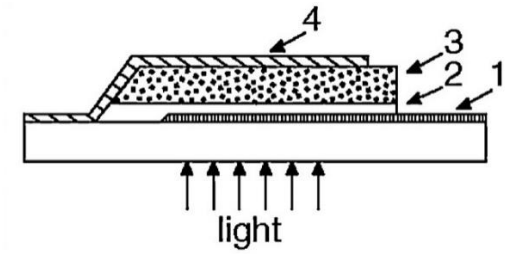

Figure 2.1.1-1. Structure of a solid-state sensitized solar cell [19]

The compact TiO_2 layer [23] is used to prevent the contact between the transparent conductive oxide (TCO) and the HTM. The two types of cells, a) and b), were illuminated with a 100 ($mW.cm^{-2}$) AM 1.5 solar simulator [22].

The J_{sc} of the $CH_3NH_3PbI_3$-based cell was 11.0 mA.cm^{-2}, much larger than that obtained for the $CH_3NH_3PbBr_3$ case (5.57 mA.cm^{-2}). V_{oc} of the cell based on lead iodide perovskite was 0.61 V much lower than for the lead bromide perovskite that was 0.96 V. The higher V_{oc} value of lead bromide can be explained by the higher ionization potential compared to the lead iodide. Also, FF is 59% for the lead bromide perovskite cell and 57% for lead iodide perovskite.

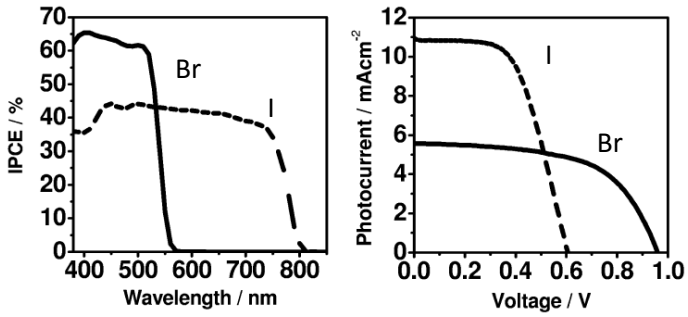

Figure 2.1.1-2. IPCE spectra (left) and photocurrent-voltage characteristics (right) for the two different perovskite sensitized solar cells [22]

Figure 2.1.1-2 shows the incident photon-to-current quantum conversion efficiency (IPCE) as function of the wavelength of the incident light, with the solid line representing the results for $CH_3NH_3PbBr_3$ and the dashed line representing the results for $CH_3NH_3PbI_3$ [22]. With the bromide perovskite the photocurrent is generated by the photon, absorbed mainly in blue-green part of the visible region while iodide perovskite allows a wider spectral responsivity, extending to λ=800 nm [22].

It is important to note that the performance of these cells decreases very rapidly over time mainly due to the contact with the environment rich in oxygen and humidity.

2.1.2. Perovskite solar cell with spiro-MeOTAD hole-transporting layer

In 2012, a group of scientists developed a new solar cell device that reached a pleasant PCE value of 9.7%. This device is based on a "photoactive layer with mesoscopic structure" where $CH_3NH_3PbI_3$ (0.395g of MAI and 1.157g of PbI_2) is inside of TiO_2 matrix, as above, and a solid hole transporting material (HTM) called spiro-MeOTAD [24].

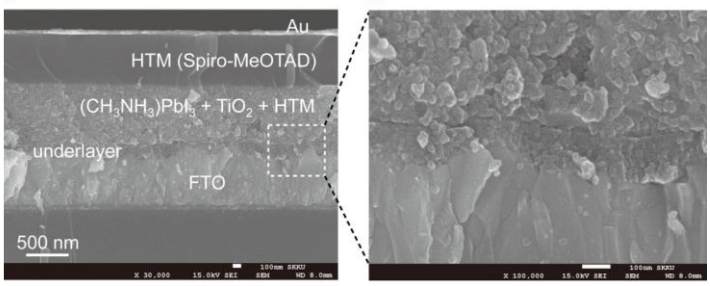

Figure 2.1.2-1. Cross section of the $CH_3NH_3PbI_3$ perovskite solar cell with the spiro-MeOTAD HTM [24]

Kim et al. concluded that J_{sc} is not strongly dependent on the thickness of the TiO_2 layer since there is a very small variation over a wide range (0.6 – 1.4 µm) of film thicknesses. However, a significant decrease of V_{oc} and FF occurs with the increase of the same film thickness. Overall, increasing the thickness of the HTM layer leads to a reduction of PCE [24].

Optimization of the device performance was obtained with a 0.6 µm thick mesoporous TiO_2 film. With these conditions they obtained a high J_{sc} of approximately 17.6 $mA.cm^{-2}$, V_{oc} of 0.88 V and FF of 62%, leading to a PCE of 9.7% [24]. Figure 2.1.2-2 shows that higher IPCE values were obtained over the wavelength range of 450 nm – 600 nm.

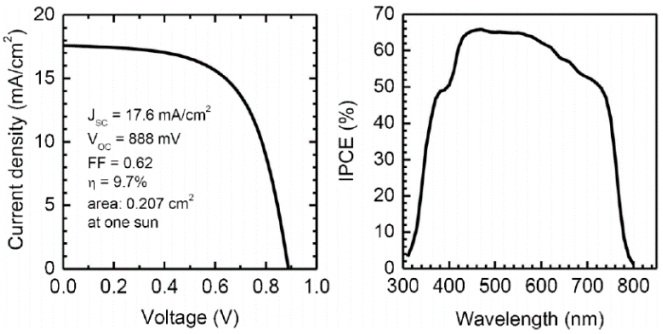

Figure 2.1.2-2. J-V curve (left) and IPCE spectra (right) characteristics of the solar cell with $CH_3NH_3PbI_3$ [24]

2.1.3. Lead perovskite solar cell with Y-TiO_2

In August 2014, a group of scientists from the University of California reached a remarkable PCE value of 19.3% (despite the cells instability) with a lead halide perovskite. This value was obtained by controlling the formation of the perovskite layer with the use of different materials suppressing carrier recombination in the absorber layer and facilitating the carrier injection into the carrier transport layers in a planar geometry without antireflective coating [21].

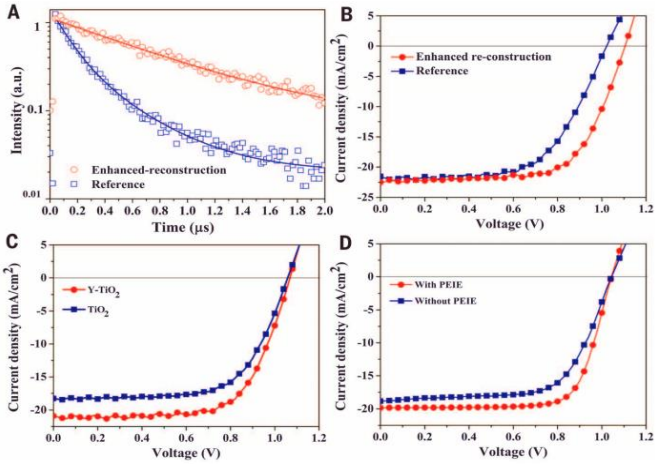

Figure 2.1.3-1. Graphic A shows photoluminescence decay curves under controlled humidity (red circles) and dry air (blue squares). Other graphics show a comparison of J-V curves in sun with reconstruction b), with Y-TiO_2 c) and with PEIE [21]

In this study they mixed two different components, $CH_3NH_3PbI_3$ and $CH_3NH_3PbCl_3$, resulting the following structure: $CH_3NH_3PbI_{3-x}Cl_x$. They also used ITO for the bottom electrode layer modified with poly-ethyleneime ethoxylated (PEIE) and yttrium-doped TiO_2 (Y-TiO_2) to enhance the extraction and transport of electrons in the EAL. They optimized the characteristics of the perovskite during film growth through careful control of the reaction between the organic and inorganic species [21].

Observing figure 2.1.3-1 it is possible to evaluate the improvement effects of re-construction deposition mechanism which consists on the perovskite deposition under controlled humidity environment (30%) b), Y-TiO2 layer c) and PEIE "incorporation" in the ITO layer d). In each of these modifications, the open-circuit voltage is higher when compared with a reference solar cell based on $CH_3NH_3PbX_3$ (X = Cl, Br, I) thin film perovskites.

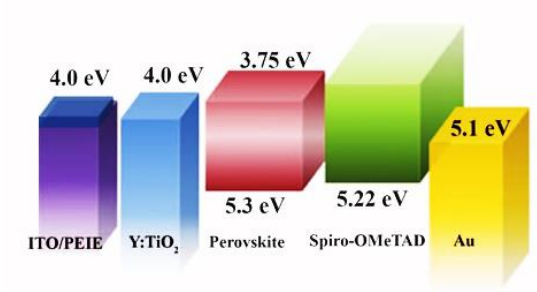

Figure 2.1.3-2. Frontier energy levels of the materials used in the modified cell [21]

Figure 2.1.3-2 show the frontier energy levels of each material used in their devices. Electrons flows from the LUMO level of perovskite to the LUMO level of Y-TiO_2 and at the same time, holes flow from the HOMO level of perovskite to the HOMO level of Spiro-OMeTAD. The addition of yttrium increases the LUMO level of TiO_2 as well as the modification of ITO with PEIE increases the LUMO level of highest work function electrode.

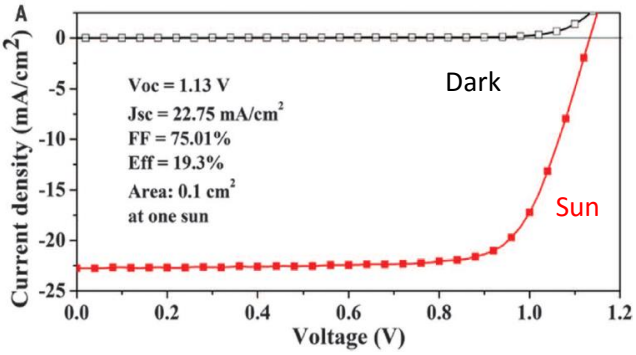

Figure 2.1.3-3. J-V curve for the improved solar cell based on $CH_3NH_3PbCl_3$ [21]

With all these optimizations they obtained the following cell parameters: V_{oc} of 1.13 V, J_{sc} of 22.75 mA.cm^{-2}, FF of 75.01% and PCE of 19.3%. All measurements were performed under a light intensity of 1 sun (100 mW.cm^{-2}) on a total surface area of 0.1 cm^2 [21].

In the same study, Zhou et al. also analyzed the stability of the perovskite samples in different storage conditions. A device stored in nitrogen glove box retained 80% of the initial performance after 1 day. After 6 days its performance decreased to 20% of the initial PCE [21]. The device stored in ambient air retained just 20% of the initial performance after 1 day and 5% after 6 days [21]. Under ambient conditions, in the presence of high levels of humidity, perovskite films undergo a faster degradation upon hydration and eventual dissolution in water environments.

We conclude that it is important to develop efficient encapsulation techniques in order to expand the use of perovskite solar cells at global scale.

2.1.4. Growth evolution of $CH_3NH_3PbI_{3-x}Cl_x$ perovskite layer

One of the most challenging factors to achieve higher PCE values is the crystallization process of perovskite films from solution.

In 2015, Liu and colleagues [25] analyzed the effect of Cl incorporation on perovskite precursor solutions promoting a controllable growth of perovskite crystals during the annealing process at 100ºC (1h).

These experiments were carried out with perovskite solution molar ratio of 1:3 ($PbCl_2$:MAI) as performed in previous works [25]. The planar solar cell structure was the following: ITO / PEDOT: PSS / Perovskite / PCBM / Ag.

In the first case they only used PbI_2 and MAI promoting a quick reaction between them and resulting in a poor coverage of surface (non-continuous perovskite film). They conclude that the presence of Cl in right proportions not only promotes good crystalline morphology but also enhances charge transport in heterojunctions [25].

After testing different molar ratios, they obtained the best results for molar ratio of 2:1:3:1 (MA:Pb:I:Cl) and a molar concentration of (0.5 M $PbCl_2$ + 0.5 M PbI_2 + 2 M MAI). This was explained not only by the good coverage of perovskite film but also by low recombination. The value for J_{sc} was 19 mA.cm^{-2}, V_{oc} of 1 V, FF was 55 % and finally PCE was approximately 12% [25]. Yet, this value was still lower than the value obtained by the structure developed by Zhou et al.

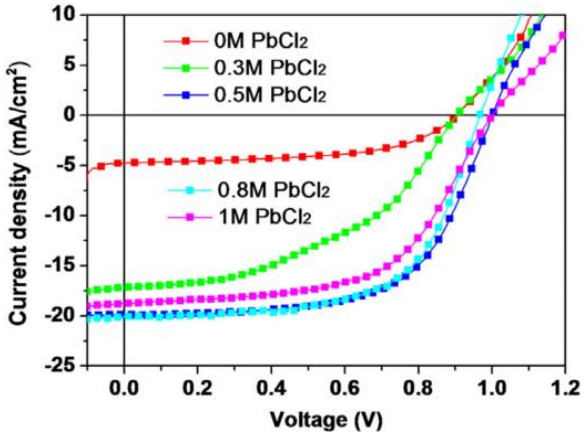

Figure 2.1.4-1. J-V curves in sun for different $PbCl_2$ molar concentrations [25]

In addition, Liu et al. tried to use an ultrathin interlayer of amino-functionalized polymer (PN4N) between the EAL and the top electrode to improve the electron transport.

The planar solar cell composition was almost the same as the previous one: ITO / PEDOT: PSS / Perovskite / PCBM / PN4N / Ag.

This interlayer increased all photovoltaic characteristics presenting considerable values: J_{sc} of 20.6 $mA.cm^{-2}$, V_{oc} of 0.98 V, FF of 77% and PCE of 15.7% [25]. This photovoltaic characterization was carried out under 1 sun illumination.

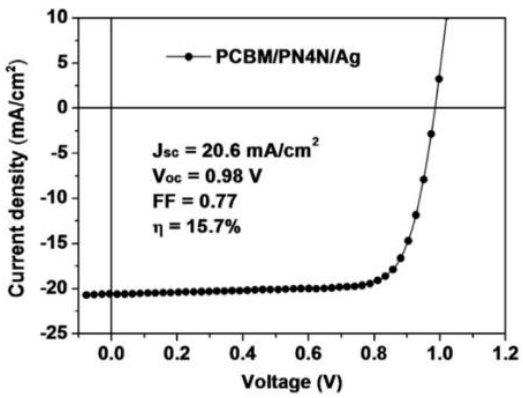

Figure 2.1.4-2. J-V curve in sun for solar cell with amino functionalized interlayer PN4N [25]

Also, in the same year, Wang et al. [26] determined the best photoactive layer thickness for $CH_3NH_3PbI_{3-x}Cl_x$ perovskite (x=2) as being approximately 575nm.

This thickness leads to a J_{sc} value of 19.8 $mA.cm^{-2}$, V_{oc} of 0.95 V, FF of 63.2% and a PCE of 11.9% [26]. This value cannot be directly compared to previous one because it does not use the same EAL materials as Liu et al. later reported to use on these devices.

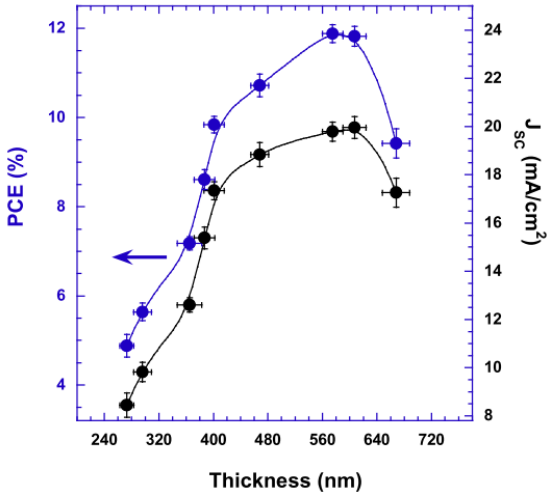

Figure 2.1.4-3. Correlation between PCE and J_{sc} for different perovskite thicknesses [26]

These values were obtained under 1 sun illumination and with the following solar cell composition [26]: ITO / PEDOT: PSS / Perovskite / $PC_{61}BM$ / Al.

2.2. Lead-free perovskite solar cells

Currently, scientists are facing the challenge to reduce environmental impacts that come from the manufacture of the perovskite photovoltaic cells. The lead components that are present in the perovskite structure are classified as “salt-like minerals” that freely dissolve in water environments or even with moisture. Also, the environmental toxicity problems related with lead manufacturing processes are a major concern [27].

2.2.1. Lead-free inorganic halide perovskite

In 2014, a group of scientists from Singapore developed lead free halide perovskite solar cells. In a first attempt, they tried to replace the Pb^{2+} ion with Sn^{2+} cation but it was completely ineffective due to the metallic nature of the layered tin perovskites. In their research they used pristine $CsSnI_3$ (inorganic equivalent of $CH_3NH_3SnI_3$) as a light absorber (also donor) due to its high optical absorption coefficient and low excitation binding energies. In a first attempt, they conclude that such material is prone to form intrinsic defects derived from Sn cation vacancies that result in metallic conductivity. Therefore, in order to overcome this problem, they added SnF_2 in different concentrations to obtain a better control of the metallic conductivity [28].

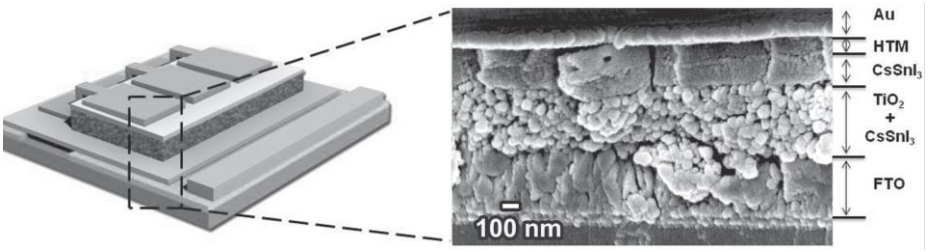

Figure 2.2.1-1. SEM image of the cross section of a solar cell with pristine $CsSnI_3$ [28]

In figure 2.2.1-1 it is possible to observe the cross-section of the perovskite solar cells image by SEM, composed by a fluorine-doped tin oxide (FTO) layer, followed by a (TiO_2+$CsSnI_3$) layer. The $CsSnI_3$ perovskite layer is then coated by a HTM layer followed by a gold electrode. In this experiment they used two different HTM layers, the 4, 4′, 4″- tris (N, N-phenyl-3-methylamino) triphenylamine (m-MTDATA) and spiro-OMeTAD. They concluded that (m-MTDATA) is energetically more beneficial than the spiro-OMeTAD due to the higher oxidation potential [28]. Also, they used dimethyl sulfoxide (DMSO) as solvent for the $CsSnI_3$ because it allows a good TiO_2 scaffold infiltration by the perovskite [28].

In these experiments they tested four amounts of tin fluoride SnF_2. They concluded that the most interesting content was for addition of 20% (SnF_2) of the total molar quantity of $CsSnI_3$ (equimolar quantities of CsI and SnI_2) [28].

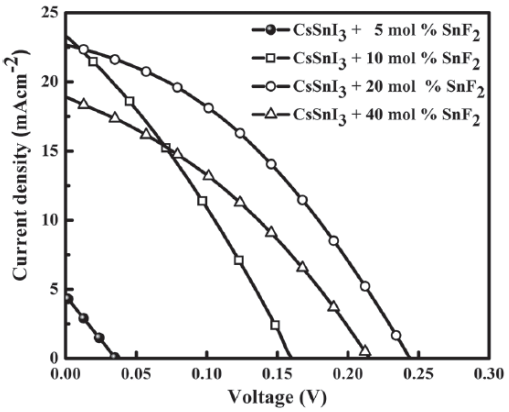

Figure 2.2.1-2. J–V curves of $CsSnI_3$-based solar cells for different amounts of SnF_2 addition [28]

Figure 2.2.1-2 shows the current density-voltage curves obtained for the different amounts of tin fluoride (SnF_2). It is important to note that the observed photocurrents are higher than for pure Sn perovskites and Pb-Sn halides.

For the solar cell with 20% SnF_2-$CsSnI_3$ they obtained, under 1 sun illumination, a V_{oc} of 0.24 V, J_{sc} of 22.70 $mA.cm^{-2}$ and a FF of 37%. The PCE obtained was 2.02% [28]. Also the spectral range of absorbed photons was located between 450 nm and 550 nm.

We observe that the results obtained with this preliminary set of experiments are quite lower than the values obtained with the lead perovskite solar cells.

2.2.2. Lead-free tin organic-inorganic perovskites solar cells

In the same year of 2014, another lead-free perovskite solar cell was developed. The most likely substitute of lead is tin (Sn), which, like lead, is a metal from the group 14 of the Periodic Table. Starting from the literature results previously obtained, a research group has tested the $CH_3NH_3SnI_3$ perovskite incorporated in a mesoporous TiO_2 scaffold. During these experiments, the authors concluded that the best results were obtained for TiO_2 thickness of 80 nm [29]. As reported in the previous work, tin can be a winning alternative over lead because it is not as toxic as lead, although the efficiencies so far obtained for tin-based cells are much lower than those of the state of the art lead perovskite solar cells [30].

Despite the similarity of tin and lead properties, because they belong to the same group, so they have the same number of valence electrons, there is a limitation to the use of this alternative element because the stability of the 2+ oxidation state decreases when we move up along the group 14 of the Periodic Table. Sn^{2+} ions are unstable towards Sn^{4+} in the presence of oxygen and moisture, thereby destroying the charge neutrality and acting like a p-type dopant (self-doping). This lower stability of Sn^{2+} in comparison with lead generates an additional problem to be overcome [29].

In order to overcome this limitation, the studies on Sn^{2+}-based salts are carried out inside a nitrogen-filled glove box [29].

$CH_3NH_3SnI_3$ is a semiconductor perovskite with an optical bandgap of 1.3 eV, which is lower than that of $CH_3NH_3PbI_3$ (1.55 eV).

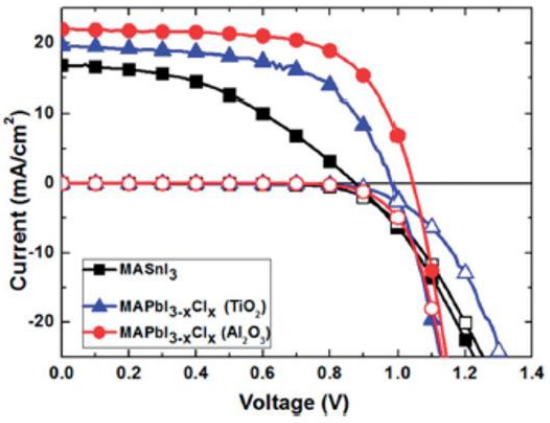

Figure 2.2.2-1. J-V curves for the Sn-based perovskite and comparison with two different Pb-based perovskites. Curves with empty symbols were obtained under dark conditions [29]

Figure 2.2.2-1 compares the photovoltaic performance for the three different devices: Pb-based devices with TiO_2 and Al_2O_3 and a Sn-based device. The values for J_{sc} obtained for the Pb-based devices were respectively 19.6 $mA.cm^{-2}$ and 21.9 $mA.cm^{-2}$ (blue and red curves). The values for V_{oc} were 0.98 V and 1.04 V, and the FF values were 60% and 66%. The corresponding power conversion efficiencies (PCE) were 11.5% e 15.0% [29]. The cells based on Sn-based perovskite and Al_2O_3 showed no photovoltaic response. The results obtained for the Sn-based perovskite solar cell with TiO_2 were: 6.4% of PCE; 0.88 V of V_{oc}; 16.8 $mA.cm^{-2}$ of J_{sc} and FF of 42% [29].

It is worth mentioning that while the use of Al_2O_3 has led to the best performing cell with the lead perovskite, it has in turn led to a non-working device when the tin perovskite was used in turn.

2.2.3. Lead-free hybrid halide tin-perovskite cells with bromide

Photovoltaic cells combining $CH_3NH_3SnI_{3-x}Br_x$ as electron donor and light harvester and HTM layer made of spiro-OMeTAD were also reported [31].

The structure of these photovoltaic cells consists on: FTO coated with mesoporous TiO_2 incorporating perovskite nanoparticles, then a spiro-OMedTAD and finally a gold electrode.

This solar cell showed the following performance parameters: V_{oc} of 0.74 V, J_{sc} of 12 $mA.cm^{-2}$, FF of 45% and a PCE of 4.44% [31].

The authors [31], also observed that the charge carriers accumulate in high density not only in TiO_2 electrodes but also in the perovskite layer. As it is known, V_{oc} is not only related with the energy difference between the HTM potential and TiO_2 conduction band but is also related with the energy difference between the HTM potential and the conduction band of the perovskite. Therefore, in order to increase the V_{oc} of these devices, bromide was added to the precursor solution to rise CB and, at the same time, increase the energy gap between both CB of donor and acceptor layers (Fig. 2.2.3-1) [31].

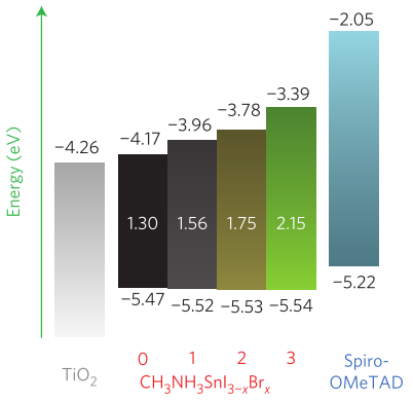

Figure 2.2.3-1. Frontier energy levels of tin perovskites with mixed Br and I content and of the hole transporting material spiro-OMeTAD [31]

Figure 2.2.3-2 shows the current density-voltage curves obtained for the devices based on the $CH_3NH_3SnI_{3-x}Br_x$ hybrid halide perovskites.

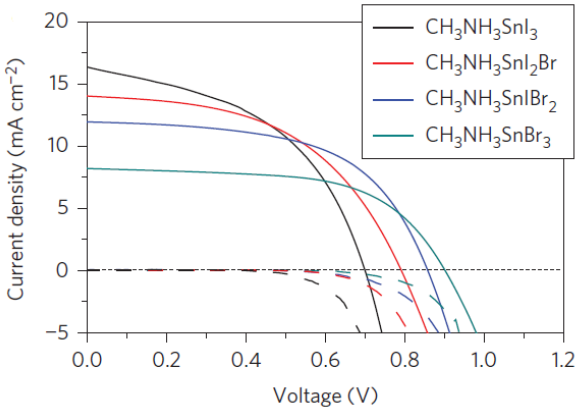

Figure 2.2.3-2. J-V curves under sunlight obtained for four different structures. Dashed lines represents J-V curves under dark conditions [31]

Among the various compositions, the perovskite structure that leads to the higher PCE (of 5.73%) is the $CH_3NH_3SnIBr_2$ with the cell showing a V_{oc} = 0.82 V, J_{sc} = 12.30 m.Acm^{-2} and FF = 57% [31].

The same authors also tested the stability of the $CH_3NH_3SnI_3$ perovskite solar cell by storing the devices in a nitrogen glove box right after sealing them with thermoforming films. During the first 12 hours, the devices lost approximately 20% of the initial performance. Hao et al. claim that these losses can be explained with a decrease in the J_{sc} and FF due to the p-type doping by some Sn^{2+} oxidation which occurred during device preparation and sealing [31].

3. Materials used in this study

The following materials were used in the fabrication of the devices: glass substrate coated with ITO, PEDOT: PSS or molybdenum oxide (MoO_3), lead- or tin-perovskite, F8T2Ox1 cross-linkable polymer, PCBM and/or C60 and bathophenanthroline (BPhen), LiF/Al contacts. The composition of each cell is detailed in section 5. During the experimental work were produced and tested more than one hundred devices with different perovskite solution compositions, different layer thickness or different electron/hole transporting layers.

3.1. Indium-tin-oxide (ITO)

The bottom contact of solar cells consists on a thin layer of indium-tin oxide (ITO, Sn-doped $In_2O_{3-\delta}$) deposited on glass. This conductive material is transparent in the visible spectral region, but almost opaque in the UV and Infra-red region [32] which makes this semiconductor a good option to be used as a transparent conducting oxide (TCO) [33].

In_2O_3 is an insulator, as it possesses a wide band gap. When Sn is added and the doping occurs, 5s electrons contribute to the modification of the electronic states at CB. As the energy-momentum dispersion remains the same as in the previous state, this makes this material a “low-carrier-concentration metal” [34] or in other words a degenerate n-type semiconductor with an optical band gap of approximately 3.7 eV and a work-function of 4.7 eV [32].

Indium-tin oxide shows low values of resistivity, ranging from 2×10^{-4} to $4 \times 10^{-4}\Omega.cm$ [35]. This can be explained with a semiconductor degeneration caused by (O_2) vacancies and substitutional (tin) dopants. In fact, it is possible to observe this phenomenon looking at the location of its Fermi level (E_F) which is close to the top of the CB [35]. ITO is widely used not only in organic photovoltaic cells (OPV) but also in organic light-emitting diodes (OLED) [35].

ITO is currently the most used transparent conducting oxide (TCO) in the optoelectronics industry [34]. A cheaper alternative is the aluminum zinc oxide (AZO) which shows a relatively good optical transmission in solar spectrum [36], although AZO is extremely sensitive to acid etching treatment and it is more degraded by moisture atmosphere which implies a relatively poor performance when compared to ITO [37].

3.2. PEDOT: PSS

One of the most used HTM layers in organic solar cells is PEDOT: PSS, a material that combines the conjugate polymer poly(3,4-ethylenedioxythiophene) and poly(styrenesulfonic acid). Polythiophenes are polymers formed by the polymerization of single thiophenes.

These conjugated polymers behave as semiconductors, and their conductivity can be largely increased by charge transfer doping, usually becoming oxidized, thereby creating free electrons over the polymer chain [38].

The acid dopes the PEDOT, which becomes oxidized, and largely increases its conductivity. The poly(styrene sulfonic acid) becomes an anionic species (composed by deprotonated sulfonyl groups). The two resulting ionomers become coulomb bound and can be dispersed in water, forming colloidal solutions [39].

Their most important properties are, high work function, high conductivity, considerable transparency and stability when doped in p-form [40]. Such properties make it a good choice to be used as part of the active layer in organic solar cells.

PEDOT:PSS has a work function above the top of the CB of the photoactive layer (containing perovskite), being widely used as HTM [40].

The following figure shows the molecular structures of PEDOT and PSS respectively.

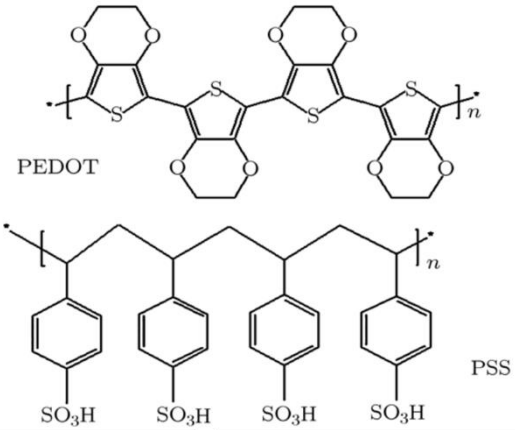

Figure 3.2-1. Molecular structures of PEDOT and PSS. Adapted from [40]

This polymer has some interesting properties, namely [41].

- Produces ohmic contacts with TCO and top electrode;
- Has a work function of 5.2 eV producing an efficient hole collection;
- It is transparent and conductive;
- Smooths the ITO substrate surface, reducing the probability of electrical shorts

3.3. Molybdenum oxide (MoO_3)

MoO_3 (molybdenum oxide) is a stable phase transition metal oxide in which the most stable oxidation state of Mo is +6. It is much less toxic when compared with other heavy metals used in photovoltaic cells. Due to its favorable energy level alignment with the active layer, it is widely used as a substitute of PEDOT: PSS to act as HTM layer.

Another advantage with the use of this material is to avoid one of the main problem of PEDOT: PSS which consists on the introduction of humidity in the samples due to its hygroscopic nature and, therefore, contributing for the ITO layer degradation [42].

This oxide buffer layer, which represents the most common molybdenum compound in its highest oxidation state, can be deposited by different PVD methods such as sputtering, thermal or electron beam evaporation [42]. This can be a possible alternative to PEDOT: PSS because of its relatively high work function (5.3 – 5.7 eV). Its semi conductive properties is due to hyper- stoichiometry produced by oxygen vacancies [43]. When mixed with bathophenanthroline (Bphen), can also be used as compound buffer for the top electrode in order to protect possible aluminum contaminations in C60 layer that arises from the Al electrode deposition [44].

3.4. Polyethylene Oxide (PEO)

Polyethylene oxide (PEO) is a thermoplastic and semicrystalline polymer [45]. It is soluble not only in water but also in a large number of organic solvents such as dimethylformamide (DMF) at room temperatures and it is also easily soluble at high temperatures in toluene and benzene [46]. This synthetic polyether has a wide range of weight average molecular weight (M_w) [47]. In case of lower molecular weight it is called polyethylene glycol (PEG), retaining PEO to designate the polymer with a molecular mass higher than $2.0x10^4$ [48]. PEO has interesting properties such as low toxicity, high melting point and low glass transition temperature [49].

The PEO used in these experiments has a weight-average molecular weight (M_w) of approximately 5.0×10^6 [46] and it can be used to enhance electron extraction from the active layer. Figure 3.3-1 shows its molecular structure.

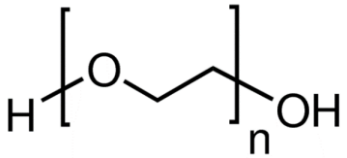

Figure 3.4-1. Molecular structure of polyethylene oxide (PEO) or polyethylene glycol (PEG) [50]

PEO incorporated in the right proportions into the precursor perovskite solution reduces perovskite crystal precipitation. This leads to a smoother and uniform photoactive layer which not only reduces the possibility of short-circuits but also promotes higher efficiency values [51]. In fact, the presence of PEO reduces the perovskite precursor diffusivity during the annealing process which induces the formation of much smaller and uniform perovskite precipitates within a PEO matrix [51].

3.5. Perovskite layer

Different perovskite compositions were used to carry out several approaches in the study of photovoltaic cells.

In the first experiments we used lead-free perovskites. We used mixtures of methyl-ammonium iodide (MAI) with tin iodide ($CH_3NH_3SnI_3$) which typically shows a HOMO energy of -4.73 eV and LUMO energy of -3.63 eV [52] and methyl-ammonium iodide with tin bromide ($CH_3NH_3SnIBr_2$) typically with HOMO energy of -5.53 eV and LUMO energy of -3.78 eV [31]. These two solutions were used to prepare the photoactive layers, with various thicknesses.

Another research was focused on the use of F8T2Ox1 as light absorber layer and methyl ammonium iodide with tin iodine ($CH_3NH_3SnI_3$) as electron acceptor layer

Trying to improve the efficiency results, SnF_2 was added to cesium iodide (C_sI+SnI_2) solution. As referred before, according to Sabba et al. the addiction of SnF_2 to methyl ammonium tin iodide should decrease the presence of vacancies, promoting higher current densities and leading to better efficiency results [53]. $CsSnI_3$ has a typically HOMO energy of -4.92 eV and LUMO energy of -3.62 eV [54].

In a second set of experiments we tested the widely used methyl-ammonium lead iodide perovskites ($CH_3NH_3PbI_3$) which has a typically HOMO energy of -5.39 eV and LUMO energy of -3.88 eV [52]. Solutions of methyl-ammonium lead iodide perovskite with polyethylene oxide (PEO) were also tested in attempting to increase the extraction of electron charges from donor film.

3.6. C_{60} / PCBM fullerene

Fullerenes are n-type organic semiconductors and can be classified as carbon-based nanoparticles with low solubility. Fullerenes are formed by 12 pentagons to close the carbon network made with a variable number of hexagons which increases the size of fullerenes. It is possible to obtain the total number of hexagons, where n represents the number of carbon atoms according to the expression (1) [55].

$$\left(\frac{2n}{2}\right) - 10 \quad (1)$$

They have also a high electron affinity which makes them a good option to be used as electron acceptor layer (EAL) in organic solar cells [56].

There are different structures of fullerenes such as spherical, tubular, ellipsoid or other forms [55]. The spherical ones are also called buckyball clusters and the smallest cage is C_{20} [57]. On the other hand, the most common molecule is C_{60}. This fullerene is used in organic solar cells as an EAL with a HOMO energy of -6.2 eV and LUMO energy of -4.5 eV [58].

Figure 3.6-1 shows the molecular structure of C_{60} and C_{20} [59].

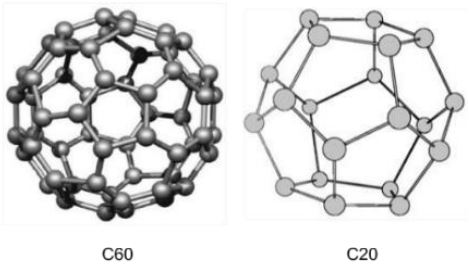

Figure 3.6-1. Molecular structures of C60 and C20 [59]

The Van der Walls diameter for individual carbon atoms in solid C_{60} molecules is estimated between 2.94 Å and 3.53 Å and the distance between the center of mass of two C_{60} neighboring units in the solid structure is approximately 10 Å [60]. They have also a carbon-carbon average bond length of 1.46 Å for bonds that combine a five-member ring with a six-member ring and an average bond length of 1.40 Å for bonds combining the two six-member rings [61].

[6,6]-phenyl-C61-butyric acid methyl ester (PCBM) is a C60 fullerene derivative. PCBM was also used as an alternative to C_{60} molecule due to its higher solubility in chlorobenzene and it shows a HOMO level at -6.2 eV and LUMO level at -3.7 eV [58] which is lower compared with LUMO level of C_{60}. The use of C_{60} as an acceptor layer promotes higher efficiencies due to its high exciton diffusion length (L_D) which is estimated between 80 - 140 Å when compared with PCBM [62].

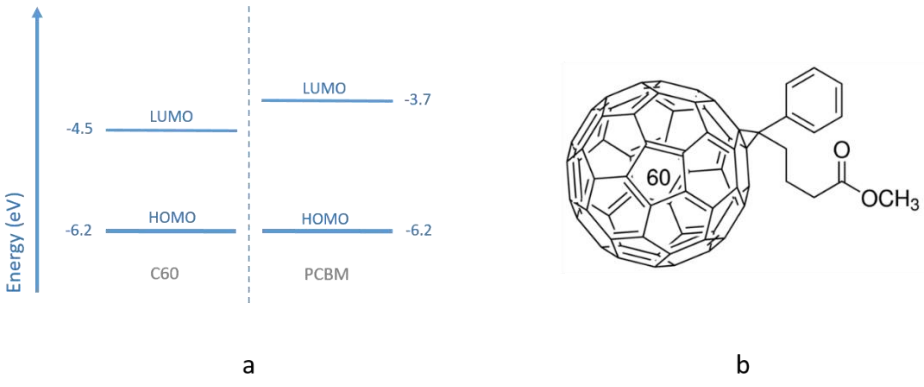

Figure 3.6-2. a) Energy diagram for C60 and PCBM. b) molecular structure of PCBM [62]

In addition to these two structures there are other conformations such as nanotubes, which are very promising materials to be used in electronic industry and other carbon-based materials [63].

3.7. Bathophenanthroline (BPhen)

Bathophenanthroline ($C_{24}H_{16}N_2$) is an organic electron transporting material widely used as buffer layer between C60 and top electrode. It shows high electron mobility of approximately 10^{-4} $cm^2/V.s$ at electric fields of 10^5 V/cm [64] and, comparing with others EAL, has low band gap with a HOMO level of -6.4 eV and LUMO level of -3 eV [65]. In view of the high surface roughness of the perovskite layer it is important to promote a regular and uniform surface to avoid direct contact with adjacent layers.

BPhen can provide a smoother buffer layer promoting a better coverage of irregular perovskite and C60 layers in order to increase the contact area and, therefore, increase the extraction of electrons to the top electrode. At the same time, this organic compound isolates the active layer from environmental gases such as oxygen diffusing mainly by the top electrode and some possible aluminum contamination that arises from Al electrode deposition [44].

According to Wang et al., the presence of an optimized thickness of BPhen can increase J_{sc} and FF, thereby improving PCE [26]. It is also important to note that BPhen has an high optical transparency in the visible region [64]. Figure 3.7-1 shows the molecular structure of BPhen.

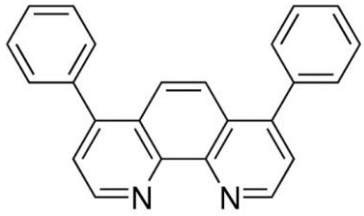

Figure 3.7-1. Molecular structure of BPhen [65]

3.8. LiF/Al electrode

In organic/inorganic non-inverted solar cells the top layer is extremely important because it works as a negative electrode extracting the negative charges that are transferred to EAL. One of the most used material in this layer is aluminum (Al) which has a work function of 4.3 eV [66]. More recently, it has been shown that it is possible to achieve higher PCE introducing a thin interlayer of lithium fluoride (LiF) under the Al electrode. Brabec et. al reported a considerable PCE increase of 20% when compared with devices without LiF interlayer [67].

There are many suggestions to explain the benefits of using the LiF interlayer such as, protection of the active layer from the incoming Al atoms during thermal evaporation deposition [67], the ability to

lower the effective work function of the Al layer and dissociation of LiF and consequent doping of the active layer [68].

Lithium fluoride is also used in OLEDs to improve the electron injection from Al. While in OLEDs, LiF allows a reduction of the electron injection barrier (from the electrode to the LUMO of the active layer), in OPV it reduces the energy barrier for the extraction of electrons leading to high efficiencies (PCE) [69].

The thickness of the LiF layer must be small (ca. 1.5 nm) in view of its electrically insulating nature. Thicker layers increase the series resistance of the device, leading to poorer performance [70].

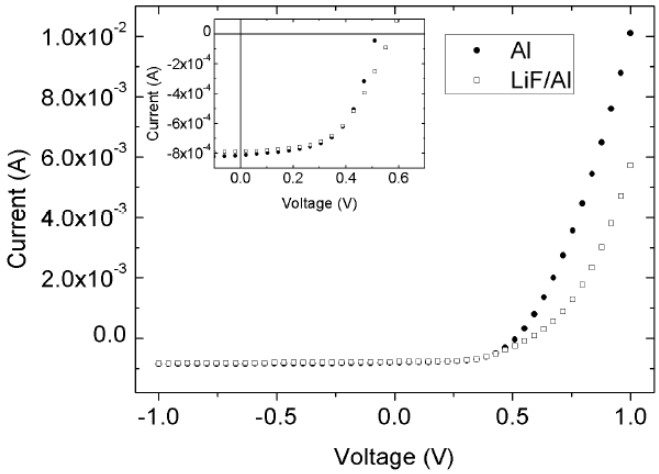

Figure 3.8-1. I-V Curves under sun illumination of two devices with and without LiF interlayer. Short graphic shows a zoom in of the I-V curves [70]

In figure 3.8-1 it is possible to observe the beneficial effect of LiF/Al (0.5 nm /100 nm) layer on V_{oc}, despite the small reduction of J_{sc} and FF, leadings to higher power conversion efficiency.

4. Experimental procedures

To produce organic/inorganic solar cells, it is essential to take into account a wide variety of fabrication steps. These OPV are composed by different layers with specific functions that congregate to the ultimate goal of higher PCE.

A variety of treatments and deposition methods was applied to the different layers: ITO, PEDOT: PSS or MoO_3, Perovskite or F8T2Ox1, C60; PCBM; BPhen and LiF/Al.

4.1. ITO etching

The first layer that composes the organic solar cells investigated in this project is a glass substrate coated with a thin layer of ITO (transparent conducting oxide). The glass/ITO substrates are cut from large plates (supplied by Visiontech) into (1.2 x 1.2) cm^2 pieces. To protect the ITO, the large plates are initially covered with fingernail polish. Glass is 1 mm thick and the ITO layer has 100 nm of thickness. which, according to Nunes de Carvalho et al. is the optimal thickness [71].

Figure 4.1-1 shows a schematic draw of the glass/ITO substrates. The ITO is etched from the sides, to avoid short circuits, leaving a central stripe, whose width (8 mm) determines the cell active area. A great effort is made to ensure that these dimensions are common to all substrates

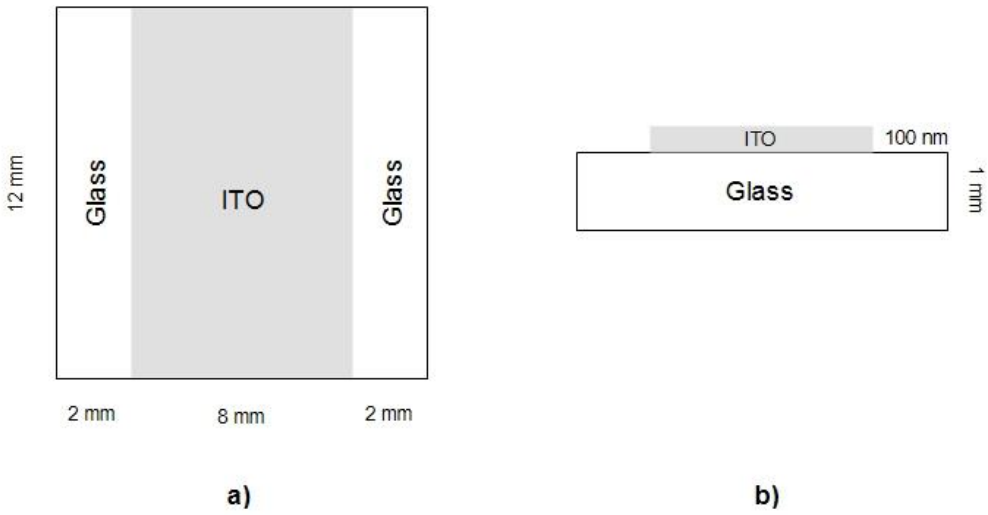

Figure 4.1-1. Schematic draw of glass/ITO substrate, a) top view and b) side view

The following steps are involved in the preparation of the glass / ITO substrates:

1. Cleaning the substrate with acetone to remove the protective nail polish.
2. Adhesive tape is placed on the sides of the ITO, leaving the central part (8 mm wide) exposed.
3. It is placed some varnish over the surface of substrates to protect the uncovered band.
4. The adhesive tape is removed after a couple of hours (to dry the varnish).
5. Substrates are placed in a beaker with diluted aqueous hydrochloric acid at solution temperature of 160 ºC for approximately 4 min to etch the ITO on the sides. Full removal can be confirmed upon measurement of the surface resistance. Caution is taken to ensure that the nail polish protecting the central stripe is not destroyed.
6. After washing with plenty of tap water, the substrates are placed in a beaker with acetone in an ultrasounds bath for 5 min to remove the nail polish.
7. The glass/ITO substrates are then thoroughly washed with detergent and distilled water under ultrasonic waves during 3 min. The procedure is repeated several times to ensure complete removal of remaining detergent.

4.2. Oxygen plasma treatment

Oxygen plasma treatment is a widely used process to clean the ITO (and other substrates) surfaces [72].

This treatment results in the formation of polar groups on the substrate surface (namely OH groups) with agents being activated by UV light or radicals [73]. As a consequence, the surface hydrophilicity is increased [74]. This treatment is very important when PEDOT: PSS is deposited on top (from an aqueous dispersion), as it allows a uniform film formation.

The samples were placed in a chamber of a plasma machine called “PlasmaPrep$_2$” under vacuum. In the second step, the O_2 bottle was opened and plasma was activated. Each treatment had a duration of approximately 3 min. In order to guarantee an efficient treatment this step was repeated another time with the same conditions. At the end of this step, the vacuum stopped, O_2 bottle was closed and the samples were removed from the chamber under atmospheric pressure. All tested samples were subjected to oxygen plasma treatment. Figure 4.2-1 shows the plasma etcher machine used in these experiments.

Figure 4.2-1. Plasma etcher machine "PlasmaPrep2"

4.3. PEDOT: PSS deposition

In some devices, PEDOT: PSS was used as hole-extracting layer, which removes the holes that are generated in the perovskite layer.

The PEDOT: PSS aqueous dispersion (purchased from Heraues with the following reference name: CLEVIOS™ PVP AI 4083 [75] was filtered with a syringe and a 0.22 μm or 0.45 μm filters, before deposition.

PEDOT: PSS deposition is performed by spin coating. This deposition method consists on depositing a particular liquid material (in this case, the conjugated polymer) on top of a spinning substrate during a short period of time. The concentration of the solution and spinning speed directly influence the thickness of the deposited layer.

To perform this deposition, substrates are putted with the desired side on top of a spin coating machine (figure 4.3-1). The vacuum generated by a connected pump assures that the substrate is fixed while spinning. Substrates were submitted to a rotation speed of 1800 rpm during approximately 45 seconds. The amount of conjugated polymer was deposited using Pasteur pipettes.

Figure 4.3-1. Spin coating machine

After this step, PEDOT: PSS layer needs to be annealed at 120 ºC on a hot plate during a period of approximately 10 min to dry the film. This procedure removes the remaining inter- and intra-particle water contained in this film [39]. The final film thickness is around 50 nm.

It should be mentioned that there are several PEDOT: PSS formulations (with different PEDOT/PSS weight ratios), that lead to films with different electrical conductivities and work-functions. Although there is a report, by Friedel et al., claiming that the optimal thickness value of PEDOT: PSS is approximately 70 nm [39], this should be taken with caution, as it will depend on the application and specific formulation.

4.4. Preparation and deposition of perovskite solutions

In order to evaluate the performance of the solar cells containing organic/inorganic perovskites, various precursor solutions were used. For each perovskite type, MAI+PbI_2, MAI+SnI_2, MAI+$SnBr_2$ and $CsSnI_3$+SnF_2 solutions with different compositions and spin coating conditions were tested in order to obtain a wide range of layer thickness and, therefore, to assess their behavior. All solutions and devices, starting from the deposition of the perovskite solutions, were prepared inside a nitrogen-filled glovebox.

4.4.1. Methyl-ammonium lead iodide (MAI+PbI_2)

Perovskite solutions with four different molar ratios of CH_3NH_3I:PbI_2 were prepared. The first set of solutions was prepared with 1:1 molar ratio of MAI:PbI_2 following several reports. The solids were then mixed in DMF, and left stirring for approximately 12h at 60 ºC. This molar ratio was tested for different solution concentrations between 30 wt% and 40 wt%. However, we could not obtain a clear solution, existing a significant amount of material in suspension.

The precursor “solution” was then deposited by spin coating at different spinning speeds during different times and submitted to different annealing conditions as shown in table 5.1.1-1.

Another three different molar ratios were tested. In these cases, there was an excess of MAI on MAI:PbI_2 molar ratios of 5:1, 1.5:1 and 1.28:1, aiming to improve the solubility. DMF was used as solvent with concentrations of 30 – 40 wt%. We found that the larger the MAI excess the clearest was the solution, suggesting that for the total solids concentration, MAI assists the PbI_2 dissolution. The 1.28:1 composition is a compromise between the aimed equimolar composition and the minimization of the amount of material in suspension. Yet, there is still some material that precipitates if the solution is left at rest at room temperature. Deposition and annealing conditions are shown in table 5.1.1-1.

Solutions of perovskite precursors (1:1 and 1.28:1) containing 6.9 mg and 13.4 mg of PEO per mass of solution were also respectively prepared. MAI was synthesized in Organic Electronics lab, PbI_2 and PEO were purchased from Sigma-Aldrich with a purity of 99%.

4.4.2. Methyl-ammonium tin-iodide (MAI+SnI_2)

Solutions with three different MAI:SnI_2 molar ratios were prepared: 0.4:1, 0.8:1 and 1:1. The solute was dissolved in DMF, with a total solids concentration between 35 wt% and 40 wt%. The solutions were left stirring for 12h at 100 ºC. In addition to the spin coating deposition, another two different deposition methods, namely doctor blade and drop cast, were tested. All deposition and annealing conditions are shown in table 5.2.1-1.

A sequential deposition process was also investigated: MAI was deposited first from an isopropanol solution and annealed for 12h at 100ºC. After 14h SnI_2 solution in DMF was deposited. The obtained precursor film was annealed for 2h at 100ºC to promote the mixing and reaction of two compounds. SnI_2 was purchased from Sigma-Aldrich with a purity of 99%.

4.4.3. Methyl-ammonium tin-iodide bromide (MAI+$SnBr_2$)

Solutions with two different MAI:$SnBr_2$ molar ratios, 0.3:1 and 2:1 were prepared in DMF with solid concentrations in the range 30-35 wt%. The precursor solutions were left stirring for approximately 12h at 100 ºC.

All deposition and annealing conditions are shown in table 5.3.1-1. $SnBr_2$ was purchased from Sigma-Aldrich with a purity of 99%.

4.4.4. Cesium tin iodide-tin fluoride ($CsSnI_3$+SnF_2)

A perovskite precursor solution with a CsI:SnI_2:SnF_2 molar ratio of 1:1:0.16 was prepared. The solute was dissolved in DMF with a concentration of 35 wt% and left stirring for 12h at 100 ºC. Deposition method and annealing conditions were the same to all devices and are shown in table 5.4.1-1.

CsI, SnI_2 and SnF_2 were purchased from Sigma-Aldrich with a purity of 99.9%, 99% and 99% respectively.

4.4.5. Deposition of perovskite solutions

Three different techniques were used to prepare thin films from the perovskite solutions on top of PEDOT: PSS or MoO_3. All the procedures were carried out in a nitrogen-filled glove box.

Spin coating was the most used method to prepare films from the perovskite solutions. This is also the most common technique to prepare thin films from solutions in general.

Drop cast was also tested aiming to improve the film quality. This technique basically consists on the deposition of a small volume of the precursor DMF solution on top of a substrate. In this case the substrate was already placed over a heating plate at a specific temperature, so that, the annealing process starts immediately after solution deposition.

Doctor Blade was the third thin film formation technique that was used. This method consists on the coating of a surface with the precursor DMF solution and subsequent removal of the solution excess with a Doctor blade (Frame), which moves along the substrate. The thickness of the layer is controlled by a gap between the doctor blade and the substrate [76]. While theoretical wet layer thickness is

referred as the distance between the doctor blade's edge and the bottom of the sample's layer, the practical wet layer is sheared due to the solution's surface tension, speed of coating and dynamic viscosity. This phenomenon promotes a practical wet layer thickness 30 % - 40 % less than the theoretical layer [76]. The following figure shows the principle of this technique.

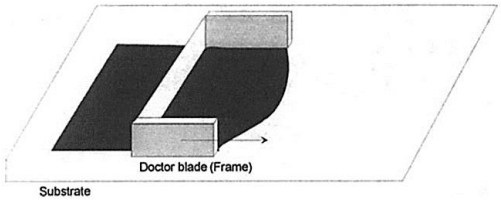

Figure 4.4.5-1. Doctor Blade deposition technique [76]

The wet layer formed on the substrate is subjected to a thermal treatment (annealing) up to 12 hours at 125 ªC - 150 ºC. This step promotes not only the removal of remaining solvent but also the crystallization of the perovskite [77]. The conversion to the final perovskite structure takes place during this process resulting in a dark brown color.

4.5. F8T2Ox1 Polymer

Another alternative to be used as the light absorber layer is the conjugated cross-linkable polymer F8T2Ox1 (oxetane-functionalized derivative of poly (9,9-dioctylfluorene-*alt*-bithiophene)). This layer is used in combination with perovskite layer which in this case represents the EAL because it has lower energy levels than F8T2Ox1 [78]. Figure 4.5-1 shows the energy levels of F8T2Ox1 and its relation with one type of perovskite ($MAPbI_3$) and PEDOT: PSS.

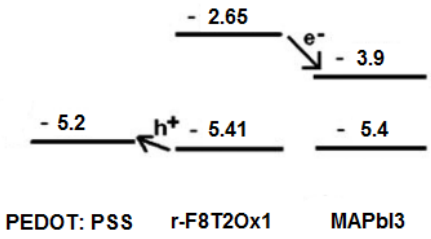

Figure 4.5-1. Energy diagram of PEDOT: PSS, F8T2Ox1 and $MAPbI_3$. Adapted from [78]

To prepare the polymer solution, 500 mg of chlorobenzene were added to 10 mg of F8T2Ox1 (synthesized in the Organic Electronics lab) and the solution was left stirring on stirrer rolls at room temperature for 24 h.

This polymer, was deposited over the PEDOT: PSS layer by spin coating at 1000 rpm during 120 s. Then it was annealed for during 2 hours at 120 ºC under vacuum conditions. This thermal treatment promotes the polymer cross-linking resulting in formation of covalent links between linear polymer chains (cross links) and creating a more rigid and stable homogeneous film.

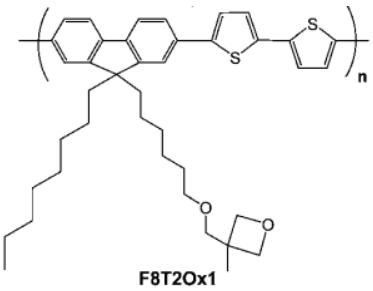

Figure 4.5-2. Chemical structure of F8T2Ox1. Adapted from [78]

4.6. Electron accepting and charge transporting layers

C60 and its soluble derivative, PCBM, were used as electron accepting materials in combination with the perovskites. The electron acceptor layer (EAL) was deposited in the same vacuum chamber that was used to deposit top contacts. The C60 layer was evaporated on top of perovskite film using the PVD method (thermal evaporation) at a base pressure of (2×10^{-6}) mbar. Deposition rate was between 0.5 and 1 Å/s to obtain a thickness of approximately 30 nm.

In PVD (thermal evaporation method), the particles to be deposited (atoms or molecules) are transformed into a gas state upon heating. Tungsten filaments are used to generate heat by the Joule effect. Organic and inorganic materials are placed inside ceramic crucibles that are heated by the tungsten filament. Once the evaporation or sublimation temperatures are reached, particles are ejected and deposited on top of the desired layer. The momentum of particles is crucial to define a good layer. If particles have a too high momentum, they can degrade the layer where they are being deposited [79].

Fullerenes - C_{60} and PCBM were purchased from Sigma-Aldrich and Solenne, respectively with a purity greater than 99% [80], [81].

The hole extraction material, MoO_3, used to replace PEDOT: PSS, was deposited by the same PVD process. Layers with thicknesses of ca. 20 nm were deposited at a rate of approximately 0.25 Å/s. Molybdenum oxide was purchased from Sigma-Aldrich with a purity of 99%.

BPhen, used as an electron transporting / hole blocking material was deposited through the same PVD method under a pressure of 2×10^{-6} mbar with a deposition rate of approximately 1 Å/s. Various thicknesses were tested. This organic material that shows a band-gap of 3.4 eV [65], was purchased from Sigma-Aldrich with a purity of 99% .

4.7. Top contact deposition

Top electrode (electron collecting) which is made with a bilayer of aluminum (Al) and lithium fluoride (LiF) was also deposited by PVD in the same system inside the glove box. Initially a thin layer of LiF (1.5 nm) [78] was thermally evaporated and then another thicker layer of Al (thicknesses above 60 nm) was evaporated on top. These materials were deposited through a shadow mask that determines, along with the ITO stripe of the bottom electrode, the device active area as 24 mm^2.

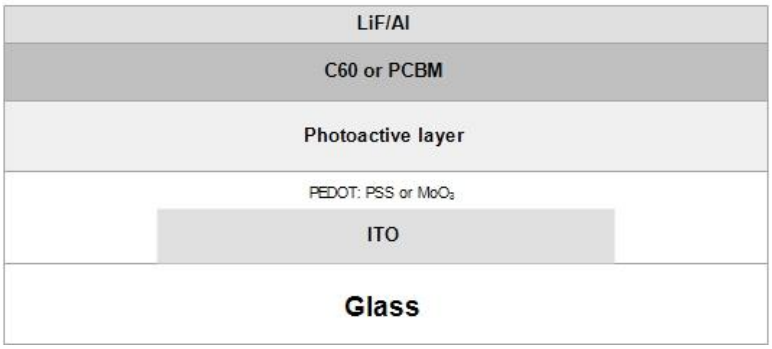

Figure 4.7-1. Cross-section of a typical photovoltaic cell produced during this work

4.8. Solar cell characterization

Solar cells were characterized under simulated solar illumination to obtain their most important parameters, short-circuit current (J_{sc}), open circuit voltage (V_{oc}), fill factor (FF) and power conversion efficiency (PCE). Illumination is provided by a solar simulator (Newport®), with a variable radiant power output, being the light intensity determined with a calibrated silicon cell. In general, a 1 sun (100 $mW.cm^{-2}$) power was used in the devices testing. The used solar simulator, consisting on a 450 W xenon lamp and a filter of class AAA [82].

The electrical characterization of the cells consisted on the measurement of their current-voltage characteristics, first in the dark and afterwards under illumination, using a K2400 source meter controlled by a computer using a homemade LabVIEW program. The current was measured as a response of voltage increments of 0.05 V in a range of -1.0 V to 1.5 V. The current density, J_{sc} is obtained by dividing the measured current by the device active area (24 mm^2).

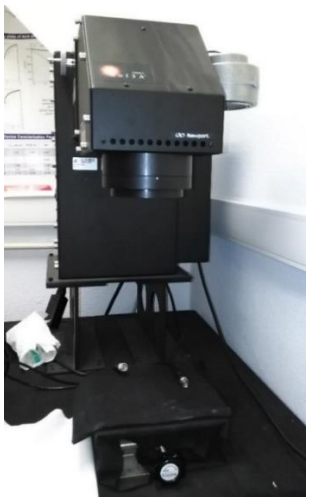

Figure 4.8-1. Solar simulator used in this study (Newport)

Figure 4.8-2 shows typical J-V curves in dark conditions. During illumination conditions, each J-V curve obtained allows to directly determine three important parameters: J_{sc}, V_{oc}, FF.

J_{sc} represents the maximum current density that is photogenerated by the cell without any bias. It is also commonly used a reverse bias current (electrons flow toward the (+) and holes flow to the (-)).

V_{oc} is the minimum voltage that we need to apply to the solar cell to nullify the photogenerated current. It is the maximum photo-voltage of the cell, corresponding to the electromotive force (emf) of a battery [83].

A third parameter used to characterize the solar cells is the fill factor (FF). This can be defined as the ideality factor of the cell, or by other words, performance ratio between the real cell and the theoretical maximum expected for that cell.

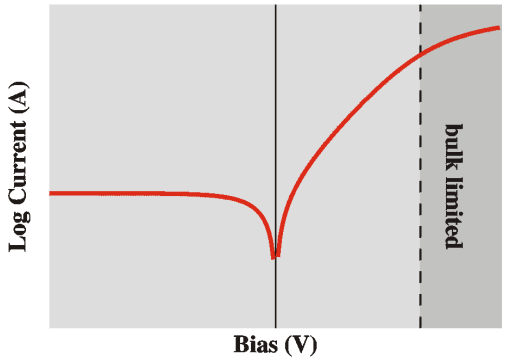

Figure 4.8-2. Typical dark current curve with rectification in logarithmic scale. Adapted from [84]

4.8.1. Spectral response and quantum efficiency

Besides the measurements of the current-voltage response of the photovoltaic cells, these are also characterized by their spectral response (R_λ). This parameter relates the generated short-circuit current density (J_{sc}) with the power of incident sunlight (P_{in}), as expressed by equation (2) for each wavelength:

$$R(\lambda) = \frac{Jsc}{Pin} \tag{2}$$

Quantum efficiency (QE) is another parameter that relates the number of electron or holes photo-generated per incident photon. If the calculation is made by taking into account the number on incident photons at each wavelength, that gives the external quantum efficiency (EQE), according equation (3):

$$QE(\lambda) = \frac{h * c * R(\lambda)}{e * \lambda} = 1240 * \frac{R(\lambda)}{\lambda} \tag{3}$$

where h represents Planck's constant, c the speed of light in vacuum, e is the electron charge and λ is the wavelength of the light beam in nm.

If the calculation is made considering the number of absorbed photons, we obtain the internal quantum efficiency (IQE). In general, due to the difficulty to determine with accuracy the number of absorbed photons (which depends not only on the absorption spectrum of the active layer but also on the filter and cavity effects), EQE is preferred.

The spectral response and quantum efficiency are obtained with a homemade system consisting essentially on a halogen lamp and a monochromator. A calibrated silicon photodetector is used to determine the number of photons impinging on the cell at each wavelength.

The sample is placed in an appropriate support; a beam light passes through a monochromator that decomposes it in different wavelengths. The sample is connected to a K2400 source meter that reads the photo-generated current without any bias applied to of the cell.

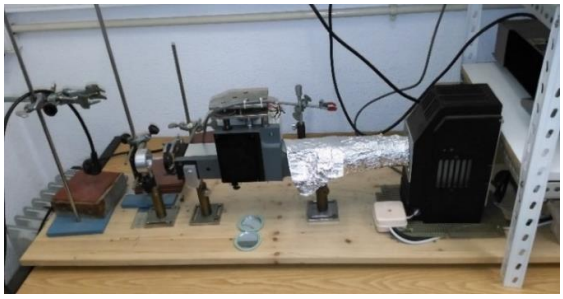

Figure 4.8.1-1. Setup to determine the spectral response of photovoltaic cells

4.8.2. Fill factor

This parameter characterizes the extraction of photo generated carriers out of the solar cell [15]. The more rectangular area fits in the J-V curve the better is the result obtained. In an ideal case, J-V curve is a rectangle representing the maximum value expected (100%). In real cases, FF cannot reach 100% not only in organic but also in inorganic photovoltaic devices. According to *Wang et. al.* the highest value reported is approximately 90%, although these values can often vary in a range between 50% and 70% [15]. This value can be obtained using equation (4):

$$FF = \frac{(Jm * Vm)Max}{Jsc * Voc} \tag{4}$$

where (J_m) Max and (V_m) Max represent the current density and open circuit voltage at the maximum power point respectively.

Many factors, such as charge extraction efficiency and recombination, contribute to FF, independently and/or in a combined way. If the space charge-limited current (SCLC) dominates the device and even if its active area is large, the charge collection at the electrodes can be insufficient to compensate the generated losses leading to a decrease of FF to the value of 25% [15]. In this case, the J-V curve deforms to a straight line resulting in the minimum square area.

4.8.3. Efficiency of solar cells

Concerning these main parameters that characterize PV cells, the ultimate goal is to obtain the maximum PCE. This can be calculated using equation (5):

$$\eta = \frac{Pm}{E * Ac} = \frac{Jsc * Voc * FF}{Pin} \tag{5}$$

where P_{in} is the light power incident on the device.

As indicated in equation (5), PCE is directly dependent on FF, J_{sc} and V_{oc}. It is usually also dependent on the illumination power (P_{in}), though the specific variation is material dependent.

One of the most important material's characteristics when aiming to obtain high power conversion efficiencies (PCE) is the energy-gap of light absorbing material. However, if the energy gap becomes too small, the ability to generate charge competes with other loss processes and the overall PCE decreases [43].

4.8.4. Films thickness determination using a surface profilometer

The thickness of each layer that composes a solar cell, in particular, the photoactive layer and charge transporting or charge blocking layers, influences the performance of these devices. If the thickness of the active layer is too small, besides inefficient light absorption, it can cause direct contact between the top and bottom electrodes resulting in a short circuit with high currents and leading to anomalous function. On the other hand, if the thickness of the active layer is too high it generates such small currents, due to the high cell resistance, that results in no function of the device. It is also important to control the thickness of the contacts and other layers that constitute all device [26], [85].

The surface contact profilometer is a rigorous instrument that analyses the film surface and measure its profile. The device uses a diamond stylus that touches the sample surface in order to generate a graph with the contours of that surface. The resolution depends on the radius of the scratch (that cuts the entire film) is made. From the surface profile across that scratch we can obtain the layer thickness from height difference between bottom and top of the layer [85].

All the thicknesses were measured with a Dektak 6M profilometer. A contact force of 1 mg was used, the scanning length was preset at several hundred microns and the scan time was 40 s.

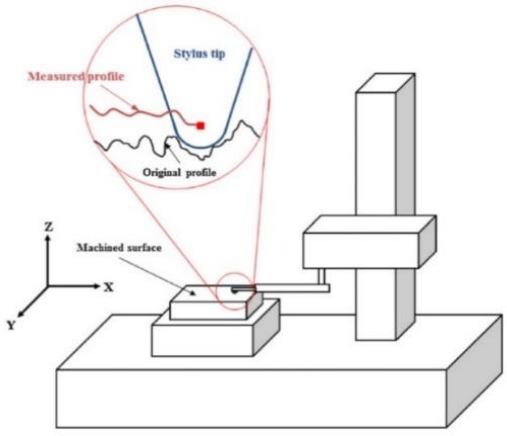

Figure 4.8.4-1. Stylus type profilometer [85]

Figure 4.8.4-2. Dektak 6M profilomenter used in this work

4.8.5. UV/Visible absorption spectra

Only the sun light that is absorbed and electronically excites the active layer can generate electric energy via the photovoltaic effect. Depending on the material in use, a portion of light can be reflected, reducing the amount of photons that are absorbed. Only a specific range of wavelength can penetrate the different layers and reach the photoactive layer.

Considering that the solar cell performance is dependent on the number of photons absorbed by the active layer, it is important to quantify not only its absorbing ability but also that of all layers making the device. For that a UV/Visible spectrophotometer is used.

UV/Visible spectroscopy is a technique used to quantify the absorption / reflectance in the ultraviolet / visible wavelength region. The energy of the photons in this wavelength region is adequate to promote electronic excitations. For a given molecule, the lower energy photon that can promote an electronic excitation corresponds to the HOMO-LUMO energy difference. If we have a material, we may also use this technique to determine its energy gap, which again corresponds to the lowest photon energy absorbed by the material in the UV/Vis range (in some inorganic semiconductors, e.g. silicon, which possess an indirect band gap, we may have an optical gap that is larger than the energy gap). This optical property is intrinsic to each material that composes all the prepared devices.

A Cecil-CE7200 UV/Vis spectrophotometer that covers the 190-900 nm wavelength range was used in this project. It has two light sources, one for the visible (a tungsten lamp) and another for the UV (a deuterium lamp).

The instrument determines, for each wavelength, the intensity of light that passes through the sample (I) and compares it to the light intensity before passing through the sample (I_0). The ratio between I and I_0 is known as transmittance (T) [86]. The absorbance can be obtained from T using equation (6) [87]:

$$\mathrm{A} = -\log\left(\frac{\mathrm{T}\%}{100\%}\right) = -\log\left(\frac{I}{I0}\right) \tag{6}$$

A spectrum is the plot of either the transmittance of absorbance as a function of the wavelength.

As mentioned above, an important material property that we may determine from its UV/Vis spectrum is the optical gap, that corresponds to the energy of the absorption onset. Equation (7) is used obtain the gap value ΔE_{Gap}.

$$\Delta E_{Gap} = \frac{1240}{\lambda} \tag{7}$$

being λ the wavelength (nm) that results from the intersection point between a tangent to the absorption peak (linear regression) and the wavelength axis.

5. Results and discussion

In this work, more than one hundred solar cells based on different perovskite solutions were produced and tested. The major difficulties faced along the project were related to the preparation of good quality perovskite films and working cells. Solutions were prepared and deposited inside the glove box to avoid humidity degradation effects. Initially, following reported solutions compositions (stoichiometric) we could not obtain proper solutions, having always solids in suspension. We have then focused on non-stoichiometric solutions of lead-based perovskite precursors. Despite the efforts, we were never able to obtain PCE values that approach those reported in literature.

Four different solutions with lead or tin were tested. Several devices were prepared with such solutions, varying the layer thickness and, organic layers combined the perovskites, and the electrode materials. The four different perovskite solutions contained MAI+SnI_2, MAI+$SnBr_2$, CsI+SnI_2+SnF_2 or MAI+PbI_2 with and without PEO. The best results obtained for each approach are summarized in this chapter.

5.1. Methyl-ammonium lead iodide ($MAPbI_3$)

5.1.1. Devices structure

Table 5.1.1-1 lists all devices based on $MAPbI_3$ that were fabricated and the average PCE obtained for each set of devices.

Devices	MAI:PbI_2 Molar ratio	Deposition method	Annealing
ITO / PEDOT: PSS / Perovskite / PCBM/ LiF/Al			
65-68	1:1	1500 rpm (18s)	100ºC (1h)
93-94	3:2	1800 rpm (30s)	100ºC (2h)
ITO / PEDOT: PSS / Perovskite / PCBM / BPhen / LiF/Al			
83-84	5:1	1800 rpm (20s)	150ºC (2h)
69-72	1:1	1500 rpm (18s)	100ºC (1h)
120-122	1.28:1	1800 rpm (15s)	100ºC (2h)
ITO / PEDOT: PSS / Perovskite / C60 / LiF/Al			
79-80	1:1	Drop cast	150ºC (2h)
77-78	1:1	1500 rpm (18s)	150ºC (2h)
ITO / MoO_3 / Perovskite / PCBM / LiF/Al			
85-88	5:1	1500/1800 rpm (20s)	100ºC (2h)
ITO / PEDOT: PSS / Perovskite / PCBM / C60 / BPhen / LiF/Al			
95-96	3:2	1800 rpm (30s)	100ºC (2h)
97-98	5:1	1800 rpm (18s)	100ºC (2h)
105-106	1.28:1	1800 rpm (15s)	100ºC (2h)
107-108 *	1.28:1	1800 rpm (15s)	100ºC (2h)
109-110	1.28:1	1800 rpm (18s)	150ºC (1h)
113-114	1.28:1	1800 rpm (15s)	100ºC (16h) **

123-128	1.3:1	1800 rpm (15s)	100ºC (2h)
ITO / PEDOT: PSS / Perovskite + PEO/ PCBM / C60 / BPhen / LiF/Al			
111-112	1.28:1	1800 rpm (15s)	150ºC (1h)
ITO / PEDOT: PSS / Perovskite + PEO/ PCBM / C60 / BPhen / Al			
101-102	5:1	1800 rpm (15s)	150ºC (1.5h)
103-104	3:2	1800 rpm (15s)	150ºC (1.5h)
ITO / PEDOT: PSS / MoO_3 / Perovskite / PCBM / C60 / BPhen / LiF/Al			
99-100	3:2	1800 rpm (18s)	100ºC (2h)
ITO / PEDOT: PSS / Perovskite / C60 / BPhen / LiF/Al			
81-82	5:1	1800 rpm (20s)	150ºC (2h)
ITO / PEDOT: PSS / PVK / Perovskite / PCBM / C60 / BPhen / LiF/Al			
129-142 ***	1.3:1	1800 rpm (15s)	100ºC (2h)

Table 5.1.1-1. Composition, deposition method and average PCE for lead perovskite-based solar cells

* Exposed for 4 min to ambient conditions to assess the humidity effect
** To study the prolonged annealing effect
*** PVK deposited at 1800 rpm with annealing at 100ºC (2h)

5.1.2. Characterization of best performing devices

Device	Jsc (mA.cm^{-2})	Voc (V)	FF (%)	PCE (%)
ITO / PEDOT: PSS / Perovskite (3:2) / PCBM / LiF/Al				
93	0.64	0.48	47.93	0.15
ITO / PEDOT: PSS / Perovskite (1.28:1) / PCBM / BPhen / LiF/Al				
122	1.14	0.32	20.48	0.07
ITO / PEDOT: PSS / Perovskite (1:1, drop cast) / C60 / LiF/Al				
79	0.30	0.48	29.33	4.20 x 10^{-2}
ITO / PEDOT: PSS / Perovskite (1.28:1) / PCBM / C60 / BPhen / LiF/Al				
105	**4.09**	**0.57**	**37.82**	**0.88**
ITO / PEDOT: PSS / MoO_3 / Perovskite (3:2) / PCBM / C60 / BPhen / LiF/Al				
99	0.14	0.32	25.10	1.12 x 10^{-2}
ITO / PEDOT: PSS / Perovskite (5:1) / C60 / BPhen / LiF/Al				
81	0.88	0.38	11.20	3.75 x 10^{-2}
ITO / PEDOT: PSS / PVK / Perovskite (1.3:1) / PCBM / C60 / BPhen / LiF/Al				
135	0.18	0.28	31.49	1.63 x 10^{-2}

Table 5.1.2-1. Parameters of the cells based on lead perovskites

5.1.3. J-V curves for the best device

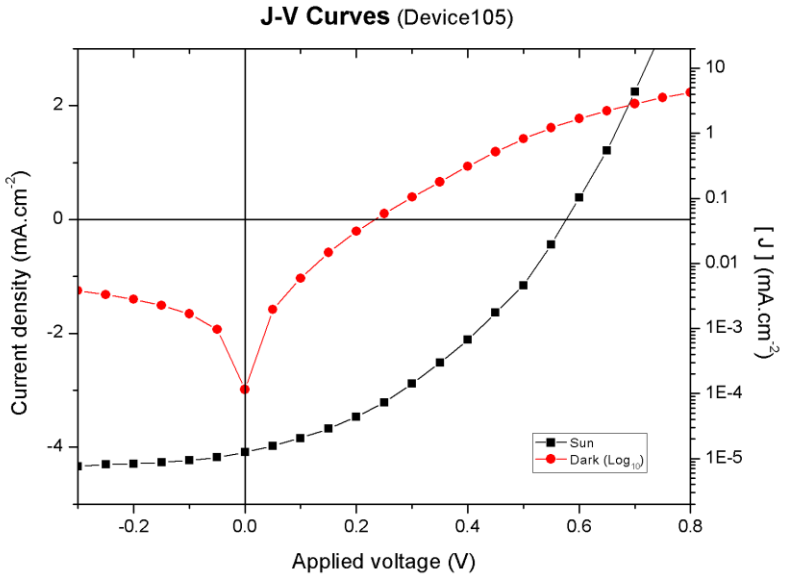

Figure 5.1.3-1. J-V curve for the best solar cell based on $MAPbI_3$ under illumination and in the dark (logarithmic scale) (Device 105)

The crystallization process induced the formation of small grains promoting a non-regular perovskite surface, accompanied by a quickly color change from yellow to dark brown.

PCBM was deposited by spin coating from a chlorobenzene solution. We found that under normal deposition conditions, the PCBM solution was dissolving the underlying perovskite layer. For that reason, PCBM solution was spin coated with the substrate already spinning to promote a fast chlorobenzene evaporation. Despite the reduction of that detrimental effect, it is likely that some of the perovskite was dissolved and removed from the substrate.

Also, four samples from this group were removed out of the nitrogen-filled glovebox to test the effect of humidity in perovskite stability [88], but also with poor results. The best result came for device 105 with a J_{sc} of 4.09 mA.cm^{-2}, V_{oc} of 0.57 V, FF of 37.82% and PCE of 0.88%. Observing the representative J-V curve it is possible to conclude that the sample exhibits a small rectification in the dark, as expected for a typical diode. These values were obtained for a spin coating deposition at 1800 rpm during 15s.

Concerning about the molar ratio, we conclude that is not appropriate to use stoichiometric compositions, preferring the use of small excess quantities of MAI in order to facilitate the dissolution of the solutes.

Observing the final results, it is possible to conclude that the incorporation of BPhen increased the PCE in all devices. Also, the use of combined C60 and PCBM as EAL promote an increase in V_{oc}, FF and PCE parameters. In fact, the mixture of these EAL materials can facilitate the electron extraction due to their combined LUMO level.

5.1.4. UV/Vis spectra of $MAPbI_3$ film

Figure 5.1.4-1 shows the absorption spectra of methylammonium lead iodide perovskite film prepared over a quartz substrate by spin coating from a 1.28:1 precursor solution. The absorptiom spectra were recorded in ambient atmosphere right after the film removal from the glove box (0 min) or after 5 min exposure to ambient atmosphere.

The absorption spans from 350 nm to 750 nm covering the entire visible spectrum. We conclude that the exposure to ambient atmosphere leads to a significant degradation, as after 5 min exposure, a slightly overall reduction in absorption is observed. The optical gap ΔE_{Gap} obtained for the spectrum at 0 min was 1.53 eV being almost unaltered after 5 min. These values are in agreement with the reported optical gaps for these perovskite [52].

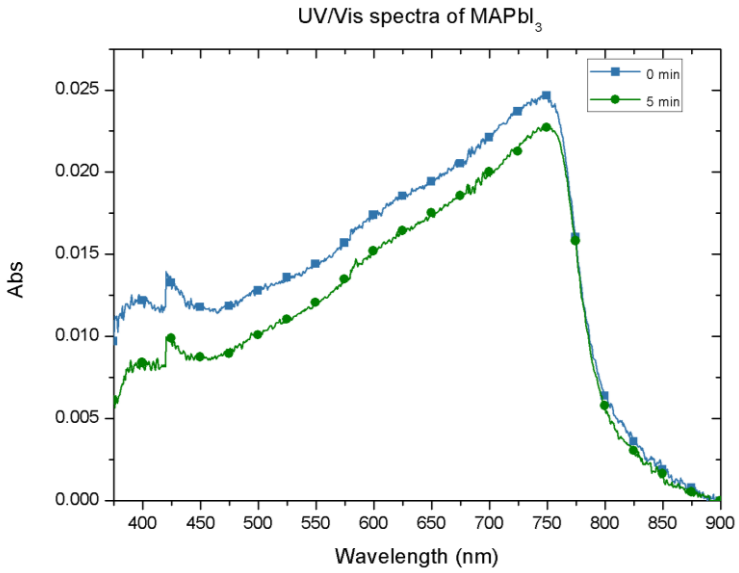

Figure 5.1.4-1. Normalized UV/Vis spectra of $MAPbI_3$ perovskite film (prepared by spin coating on a quartz substrate from a 1.28:1 solution)

5.2. Methyl-ammonium tin iodide ($MASnI_3$)

5.2.1. Devices structure

Approximately thirty samples with methyl ammonium tin iodide were prepared. On these different samples were tested two different molar ratios with three different deposition methods of perovskite for the same structure device presented on table 5.2.1-1. Were also tested diverse annealing temperatures with different times to evaluate and compare the behavior of each sample.

Devices 73 and 74 used Bphen (60 nm) and devices 75 and 76 used Bphen (6 nm) in order to improve PCE but the results remained very poor.

Also, sequential deposition of SnI_2 and MAI in samples 25 to 32 was performed, but it did not promote better result [89]. Four samples with F8T2Ox1 polymer as donor layer and perovskite as acceptor layer were tested but this did not resulted in better values either. The crystallization process promoted again irregular perovskite surfaces.

Table 5.2.1-1 lists all devices based on $MASnI_3$ that were fabricated and the average PCE obtained for each set of devices.

Devices	MAI:SnI_2 Molar ratio	Deposition method	Annealing
ITO / MoO_3 / Perovskite / C60 / LiF/Al			
21-22	0.4:1	1000 rpm (15s)	100ºC (2h)
25-28 *	0.4:1	1000 rpm (15s)	110ºC (2h)
ITO / PEDOT: PSS / Perovskite / C60 / LiF/Al			
29-30 *	0.4:1	2500 rpm (15s)	100ºC (2h)
31-32 *	0.4:1	6000 rpm (18s)	100ºC (2h)
33-34 **	0.4:1	6000 rpm (18s)	100ºC (2h)
35-36	0.4:1	1000 rpm (15s)	115ºC (1.5h)
37-38	0.4:1	3000 rpm (15s)	115ºC (2h)
45-46	0.4:1	Doctor Blade	100ºC (2h)
47-48	0.4:1	Drop Cast	100ºC (2h)
57-60	1:1	1500 rpm (30s)	100ºC (2h)
ITO / PEDOT: PSS / Perovskite / C60 / BPhen / LiF/Al			
73-74	0.8:1	1500 rpm (18s)	100ºC (1h)
75-76	0.8:1	1500 rpm (18s)	100ºC (1h)

Table 5.2.1-1. Composition, deposition method and average PCE for $MASnI_3$ solar cells

* Sequential deposition of SnI_2 and then MAI at 100ºC.
** Duplication volume from previous solution to decrease its concentration and reduce thickness layer.

5.2.2. Characterization of best performing devices

Device	Jsc ($mA.cm^{-2}$)	Voc (V)	FF (%)	PCE (%)
ITO / MoO_3 / Perovskite (0.4:1) / PCBM / LiF/Al				
21	0.61	0.01	--	--
ITO / PEDOT: PSS / Perovskite (1:1) / C60 / LiF/Al				
59	0.26	0.13	25.57	8.30×10^{-3}
ITO / PEDOT: PSS / Perovskite (0.8:1) / C60 / BPhen / LiF/Al				
74	0.17	0.08	--	--

Table 5.2.2-1. Parameters of the cells based on $MASnI_3$ solar cell

5.2.3. J-V curves for the best device

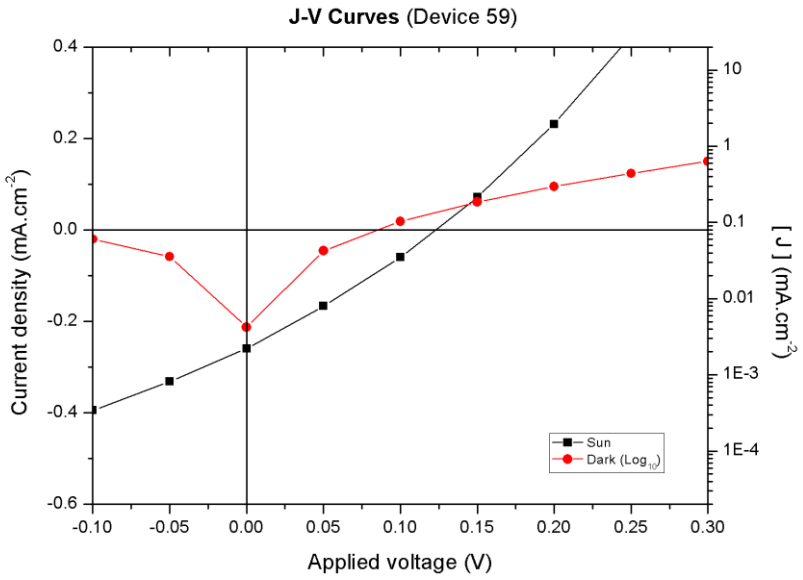

Figure 5.2.3-1. J-V curve for the best solar cell based on $MASnI_3$ under illumination and in the dark (logarithmic scale) (Device 59)

Observing the final results, we can conclude that the use of BPhen did not promote better results. Also, the stoichiometric composition resulted in the most favorable parameters. The use of C60 promoted better V_{oc} values which is preferable over PCBM material.

Device 59 had the best results with a J_{sc} of 0.26 $mA.cm^{-2}$, V_{oc} of 0.13 V, FF of 25.57% and PCE of 8.30 x 10^{-3} %. These results were obtained with spin coating deposition at 1500 rom during 30s.

5.3. Methyl-ammonium tin iodide-bromide ($MASnIBr_2$)

5.3.1. Devices structure

Table 5.3.1-1 lists all devices based on $MASnIBr_2$ that were fabricated and the average PCE obtained for each set of devices.

Devices	MAI:$SnBr_2$ Molar ratio	Deposition method	Annealing
		ITO / MoO_3 / Perovskite / C60 / LiF/Al	
23-24	0.3:1	1500 rpm (18s)	100ºC (2h)
		ITO / PEDOT: PSS / Perovskite / C60 / BPhen / LiF/Al	
115-116	2:1	2000 rpm (25s)	120ºC (2h)
117-118	2:1	2400 rpm (25s)	120ºC (2h)

Table 5.3.1-1. Composition, deposition method and average PCE for $MASnIBr_2$ solar cells

5.3.2. Characterization of best performing devices

Device	Jsc (mA.cm^{-2})	Voc (V)	FF (%)	PCE (%)
ITO / MoO_3 / Perovskite (0.3:1) / C60 / LiF/Al				
23	0.38	0.006	--	--
ITO / PEDOT: PSS / Perovskite (2:1) / C60 / BPhen / LiF/Al				
115	0.33	0.24	25.86	2.00 x 10^{-2}

Table 5.3.2-1. Parameters of the cells based on $MASnIBr_2$ solar cell

5.3.3. J-V curves for the best device

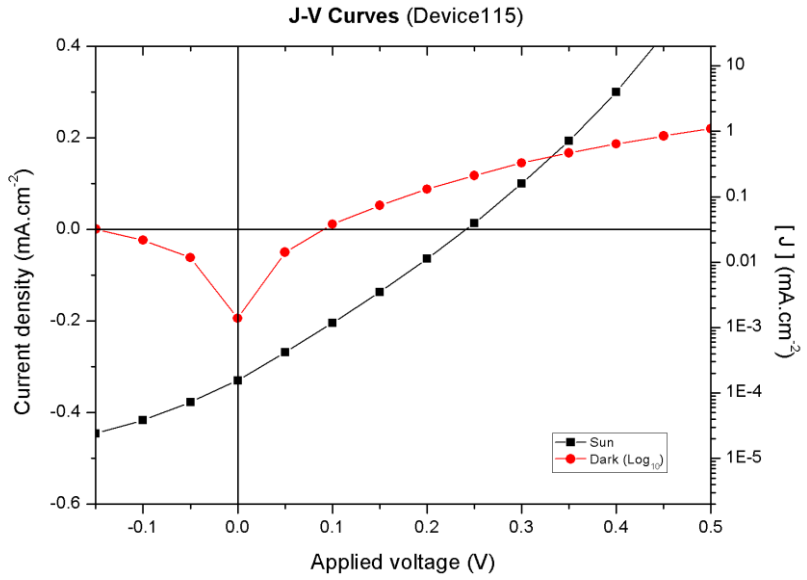

Figure 5.3.3-1. J-V curve for the best solar cell based on $MASnIBr_2$ under illumination and in the dark (logarithmic scale) (Device 115)

To evaluate the behavior of tin bromide in perovskite solution were prepared approximately ten samples. Were tested two different molar ratios with the same deposition method but with different times and spinning speeds in order to determine the effect of the perovskite layer thickness. Despite of the thicknesses were not measured as these modifications did not promote considerable changes on the parameters, all deposition conditions promoted films with a thickness range of 200-300 nm as reported in literature [85]. The annealing temperature was maintained between 100ºC and 120ºC during the same period of time. Devices 115 to 118 contained BPhen to improve the efficiency results. Once again, it was not possible to obtain smooth perovskite surfaces as reported in literature.

Among the various devices tested, the best performing device (115) showed a J_{sc} of 0.33 mA.cm^{-2}, V_{oc} of 0.24 V, FF of 25.86% and PCE of 2.00 x 10^{-2} %. The J-V curve in dark did not showed significant rectification. The previous values were obtained with a deposition performed by spin coating technique at 2000 rpm during 25s.

5.4. Cesium tin iodide perovskite with tin fluoride ($CsSnI_3$+SnF_2)

5.4.1. Devices structure

Table 5.4.1-1 lists all devices based on $CsSnI_3$+SnF_2 that were fabricated and the average PCE obtained for each set of devices.

Devices	CsI:SnI_2:SnF_2 Molar ratio	Deposition method	Annealing
ITO / PEDOT: PSS / Perovskite / C60 / LiF/Al			
49-52	1:1:0.16	1500 rpm (25s)	100ºC (2h)
ITO / PEDOT: PSS / Perovskite / PCBM / LiF/Al			
53-56	1:1:0.16	1500 rpm (25s)	100ºC (2h)
61-64	1:1:0.16	1500 rpm (30s)	100ºC (2h)

Table 5.4.1-1. Composition, deposition method and average PCE for solar cells based on $CsSnI_3$ doped with SnF_2

5.4.2. Characterization of best performing devices

Device	Jsc (mA.cm^{-2})	Voc (V)	FF (%)	PCE (%)
ITO / PEDOT: PSS / Perovskite (1:1:0.16) / C60 / LiF/Al				
49	1.01	0.01	--	--
ITO / PEDOT: PSS / Perovskite (1:1:0.16) / PCBM / LiF/Al				
63	0.23	0.07	19.60	3.16 x 10^{-3}

Table 5.4.2-1. Parameters of the cells based on $CsSnI_3$+SnF_2 solar cell

5.4.3. J-V curves for the best device

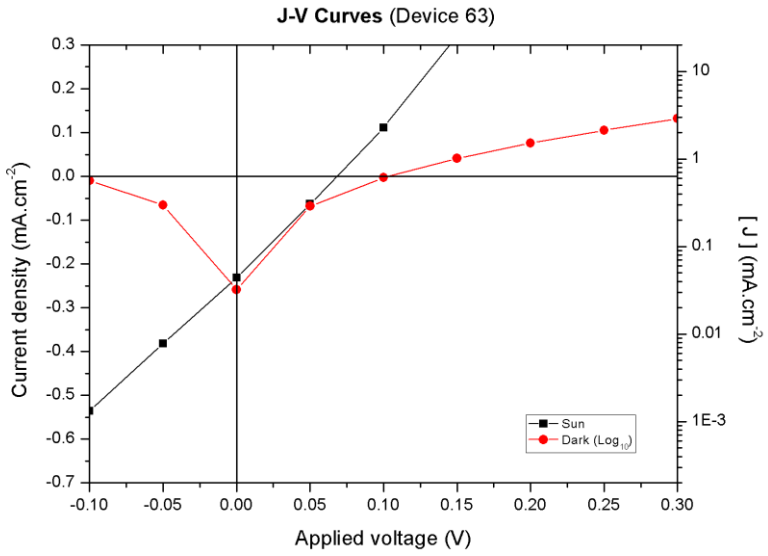

Figure 5.4.3-1. J-V curve for the best solar cell based on $CsSnI_3$+SnF2 under illumination and in the dark (logarithmic scale (Device 63)

Approximately fifteen samples of these solar cell type were prepared. The molar ratio used was the same for all devices as well the conditions of deposition method and annealing process. Also the structure used was the same on all devices, except for the use of either C60 or PCBM as electron acceptor. Due to the poor results presented by this type of photovoltaic cells, no further studies were carried out. Both J_{sc} and V_{oc} were very small which led to very small PCE values.

Also, the presence of tin fluoride apparently did not promote an increase of free charges as it did not show higher J_{sc} and V_{oc} values as expected.

The best result with this perovskite composition was obtained from device 63 with a J_{sc} of 0.23 mA.cm-2, V_{oc} of 0.07 V, FF of 19.60% and PCE of 3.16 x 10^{-3} %. Once again, current-voltage in the dark did not show any rectification, meaning that for the devices fail to show a typical behavior of a diode. The preferred deposition technique was spin coating at 1500 rpm during 30s.

6. Conclusions

During this project we prepared and tested more than one hundred photovoltaic cells with four different types of perovskites; $MAPbI_3$; $MASnI_3$; $MASnIBr_3$; $CsSnI_3$+SnF_2. All solutions were prepared and deposited in a nitrogen-filled glove box.

For each perovskite composition films were prepared various layer thicknesses, methods of deposition, temperature and annealing times.

In global terms, all the obtained results remained well below the values reported in literature. The max reported PCE (21%) for lead-perovskites was obtained by Grätzel et al. in December 2015 [90]. The best result was obtained for device 105 with a donor layer of $MAPbI_3$ hole extracting layer made of PEDOT: PSS, and electron acceptor/transporting layer composed by PCBM, C60 and BPhen. The PCE obtained with this device was 0.88 % with a J_{sc} of 4.09 $mA.cm^{-2}$, V_{oc} of 0.57 V and a FF of 37.82 %.

The main difficult faced during this work was the preparation of both clear solutions (without suspended materials) and good quality films, leading to devices without short circuits. The majority of devices contained perovskite layers with only small grains which does not show a good crystallization and resulting in irregular surfaces which not completely cover the bellower layers (Figure 6-1, a). Also, this phenomenon can be visible through a sudden change in perovskite color from yellow to dark brown resulting from the quickly crystallization.

All devices showed dark J-V curves with small or non-rectification. Rectification is expected for a p-n junction diode which leads to the conclusion that, even in the dark, solar cells do not exhibit a typical diode behavior. It is therefore not surprising that we failed to obtain good performances, when comparing with those reported in the literature. As referred in literature, a possibility of improvement would be the perovskite precursor solutions filtration prior to deposition in order to reduce the size of the particles in suspension. Although, this attempt only reduces the amount of non-soluble perovskite promoting a modification of initial molar ratio which is not desirable.

These studies, though failing to provide photovoltaic cells with high efficiencies, provided a research direction, namely the optimization of the molar ratio between methyl ammonium (MAI) and the other perovskite component once we observed that excess MAI is needed in order to promote a complete dissolution of the lead and tin salts in DMF. Furthermore, the right thickness of the electron donor layer greatly influences PCE and needs to be optimized.

Combining these solution preparation improvements with novel heterojunction surface morphologies between donor and acceptor layers, we believe that it will be possible to reach better PCE results.

Nowadays, photovoltaic industry is facing an incredible fast growing mainly in the organic area providing more and better solutions to a market increasingly dependent on energy needs.

Its applications continue growing and no longer just go through the basic needs that fostered its development but also progressively enhance a sustainable future technological grow.

From Space to Earth, major industry will increasingly need this type of renewable energy not only at short but also at medium term.

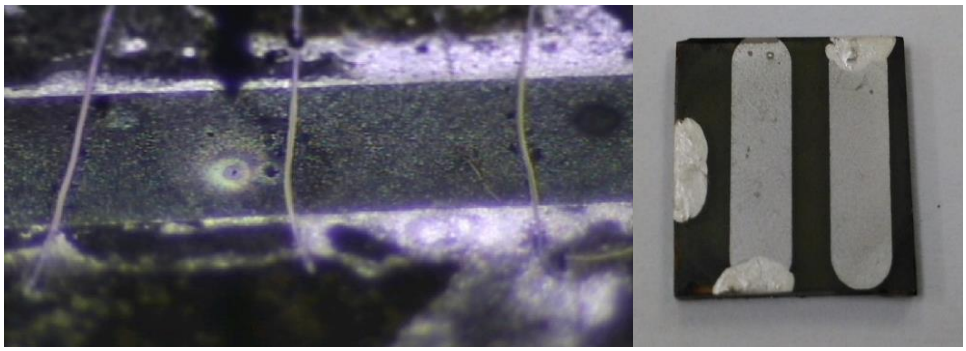

a) **b)**

Figure 6-1. a) Irregular perovskite film surface. b) $MAPbI_3$ perovskite solar cell

References

[1] G. Crabtree, E. Kocs, and T. Aláan, “Energy, society and science: The fifty-year scenario,” *Futures*, vol. 58, pp. 53–65, Apr. 2014.

[2] PORDATA, “Consumidores de electricidade: total e por tipo de consumo - Portugal,” 2012. [Online]. Available: http://www.pordata.pt/Portugal/Ambiente+de+Consulta/Tabela. [Accessed: 10-Nov-2014].

[3] T. C. Sum and N. Mathews, “Advancements in perovskite solar cells: photophysics behind the photovoltaics,” *Energy Environ. Sci.*, vol. 7, no. 8, pp. 2518–2534, May 2014.

[4] L. D. P. Lewis M. Fraas, *Solar Cells and Their Applications*. Wiley, 2010.

[5] U.S. Department of Energy, “The History of Solar,” 2014. [Online]. Available: https://www1.eere.energy.gov/solar/pdfs/solar_timeline.pdf. [Accessed: 05-Dec-2014].

[6] F. Jay, D. Muñoz, T. Desrues, E. Pihan, V. Amaral de Oliveira, N. Enjalbert, and A. Jouini, “Advanced process for n-type mono-like silicon a-Si:H/c-Si heterojunction solar cells with 21.5% efficiency,” *Sol. Energy Mater. Sol. Cells*, vol. 130, pp. 690–695, Nov. 2014.

[7] The Economist, “Sunny uplands,” 2013. [Online]. Available: http://www.economist.com/news/21566414-alternative-energy-will-no-longer-be-alternative-sunny-uplands. [Accessed: 05-Dec-2014].

[8] E. Baker, M. Fowlie, D. Lemoine, and S. S. Reynolds, “The Economics of Solar Electricity,” *Annu. Rev. Resour. Econ.*, vol. 5, no. 1, pp. 387–426, Jun. 2013.

[9] W. G. J. H. M. van Sark, G. W. Brandsen, M. Fleuster, and M. P. Hekkert, “Analysis of the silicon market: Will thin films profit?,” *Energy Policy*, vol. 35, no. 6, pp. 3121–3125, Jun. 2007.

[10] M. Jamil, S. Kirmani, and M. Rizwan, “Techno-Economic Feasibility Analysis of Solar Photovoltaic Power Generation: A Review,” *Smart Grid Renew. Energy*, vol. 03, no. 04, pp. 266–274, 2012.

[11] G. Barbose, N. Darghouth, S. Weaver, and R. Wiser, “Tracking the Sun VI An Historical Summary of the Installed Price Tracking the Sun VI An Historical Summary of the Installed Price of Photovoltaics in the United States from 1998 to 2012,” no. July, p. 70, 2013.

[12] D. Bera, L. Qian, T.-K. Tseng, and P. H. Holloway, “Quantum Dots and Their Multimodal Applications: A Review,” *Materials (Basel).*, vol. 3, no. 4, pp. 2260–2345, Mar. 2010.

[13] M. Tao, “Inorganic Photovoltaic Solar Cells: Silicon and Beyond,” *Electrochem. Soc. Interface*, vol. 17, pp. 30–35, 2008.

[14] J. M. T. Pereira, “Semicondutores,” in *Fundamentos de Electrónica*, Lisboa, 2010, pp. 1–68.

[15] B. Qi and J. Wang, “Fill factor in organic solar cells,” *Phys. Chem. Chem. Phys.*, vol. 15, pp. 8972–8982, Aug. 2013.

[16] J. T. Calow, P. J. Deasley, S. J. T. Owen, and P. W. Webb, “A review of semiconductor heterojunctions,” *J. Mater. Sci.*, vol. 2, no. 1, pp. 88–96, Jan. 1967.

[17] S. S. Mahajan, A. Dhaul, R. Laishram, S. Kapoor, S. Vinayak, and B. K. Sehgal, “Micro-structural evaluation of Ti/Al/Ni/Au ohmic contacts with different Ti/Al thicknesses in AlGaN/GaN HEMTs,” *Mater. Sci. Eng. B*, vol. 183, no. 1, pp. 47–53, Apr. 2014.

[18] S. De Wolf, A. Descoeudres, Z. C. Holman, and C. Ballif, “High-efficiency Silicon Heterojunction Solar Cells: A Review,” *Green*, pp. 7–24, Jan. 2012.

[19] N.-G. Park, “Perovskite solar cells: an emerging photovoltaic technology,” *Mater. Today*, vol. 18, no. 2, pp. 65–72, Mar. 2015.

[20] W. J. Yin, J. H. Yang, J. Kang, Y. Yan, and S. H. Wei, “Halide perovskite materials for solar cells: a theoretical review,” *J. Mater. Chem. A*, vol. 3, no. 17, pp. 8926–8942, 2015.

[21] H. Zhou, Q. Chen, G. Li, S. Luo, T. B. Song, H. S. Duan, Z. Hong, J. You, Y. Liu, and Y. Yang, “Interface engineering of highly efficient perovskite solar cells,” *Science (80-.).*, vol. 345, no. 6196, pp. 542–546, Aug. 2014.

[22] A. Kojima, K. Teshima, Y. Shirai, and T. Miyasaka, “Organometal Halide Perovskites as Visible-Light Sensitizers for Photovoltaic Cells,” *J. Am. Chem. Soc.*, vol. 131, no. 17, pp. 6050–6051, May 2009.

[23] A. J. Frank, N. Kopidakis, and J. Van De Lagemaat, “Electrons in nanostructured TiO2 solar cells: transport, recombination and photovoltaic properties,” *Coord. Chem. Rev.*, vol. 248, no. 13–14, pp. 1165–1179, Jul. 2004.

[24] H. S. Kim, C. R. Lee, J. H. Im, K. B. Lee, T. Moehl, A. Marchioro, S. J. Moon, R. Humphry-Baker, J. H. Yum, J. E. Moser, M. Grätzel, and N. G. Park, “Lead Iodide Perovskite Sensitized All-Solid-State Submicron Thin Film Mesoscopic Solar Cell with Efficiency Exceeding 9%,” *Sci. Rep.*, vol. 2, pp. 1–7, Aug. 2012.

[25] J. Liu, J. Lin, Q. Xue, Q. Ye, X. He, L. Ouyang, D. Zhuang, C. Liao, H. L. Yip, J. Mei, and W. M. Lau, “Growth and evolution of solution-processed CH3NH3PbI3-xClx layer for highly efficient planar-heterojunction perovskite solar cells,” *J. Power Sources*, vol. 301, pp. 242–250, Jan. 2015.

[26] K. Wang, C. Liu, P. Du, L. Chen, J. Zhu, A. Karim, and X. Gong, “Efficiencies of perovskite hybrid solar cells influenced by film thickness and morphology of CH3NH3PbI3−xClx layer,” *Org. Electron.*, vol. 21, no. February, pp. 19–26, Jun. 2015.

[27] J. Yoo, S. B. Kim, W. K. Kim, and J. Jung, “Toxicity identification of effluent from a semiconductor lead frame manufacturing factory,” *J. Ind. Eng. Chem.*, vol. 20, no. 2, pp. 494–498, Mar. 2014.

[28] M. H. Kumar, S. Dharani, W. L. Leong, P. P. Boix, R. R. Prabhakar, T. Baikie, C. Shi, H. Ding, R. Ramesh, M. Asta, M. Graetzel, S. G. Mhaisalkar, and N. Mathews, “Lead-Free Halide Perovskite Solar Cells with High Photocurrents Realized Through Vacancy Modulation,” *Adv. Mater.*, vol. 26, no. 41, pp. 7122–7127, Nov. 2014.

[29] N. K. Noel, S. D. Stranks, A. Abate, C. Wehrenfennig, S. Guarnera, A. A. Haghighirad, A. Sadhanala, G. E. Eperon, S. K. Pathak, M. B. Johnston, A. Petrozza, L. M. Herz, and H. J. Snaith, “Lead-free organic–inorganic tin halide perovskites for photovoltaic applications,” *Energy Environ. Sci.*, vol. 7, no. 9, pp. 3061–3068, May 2014.

[30] P. Qin, S. Tanaka, S. Ito, N. Tetreault, K. Manabe, H. Nishino, M. K. Nazeeruddin, and M. Grätzel, “Inorganic hole conductor-based lead halide perovskite solar cells with 12.4% conversion efficiency,” *Nat. Commun.*, vol. 5, May, pp. 1–6, May 2014.

[31] F. Hao, C. C. Stoumpos, D. H. Cao, R. P. H. Chang, and M. G. Kanatzidis, “Lead-free solid-state organic–inorganic halide perovskite solar cells,” *Nat. Photonics*, vol. 8, no. 6, pp. 489–494, May 2014.

[32] A. M. Gheidari, E. A. Soleimani, M. Mansorhoseini, S. Mohajerzadeh, N. Madani, and W. S. Kolahi, “Structural properties of indium tin oxide thin films prepared for application in solar cells,” *Mater. Res. Bull.*, vol. 40, no. 8, pp. 1303–1307, 2005.

[33] M. S. Farhan, E. Zalnezhad, A. R. Bushroa, and A. A. D. Sarhan, “Electrical and optical properties of indium-tin oxide (ITO) films by ion-assisted deposition (IAD) at room temperature,” *Int. J. Precis. Eng. Manuf.*, vol. 14, no. 8, pp. 1465–1469, 2013.

[34] J. J. Lin and Z. Q. Li, “Electronic conduction properties of indium tin oxide: single-particle and many-body transport,” *J. Phys. Condens. Matter*, vol. 26, no. 34, p. 1-21, 2014.

[35] H. Kim, C. M. Gilmore, A. Piqué, J. S. Horwitz, H. Mattoussi, H. Murata, Z. H. Kafafi, and D. B. Chrisey, “Electrical, optical, and structural properties of indium–tin–oxide thin films for organic light-emitting devices,” *J. Appl. Phys.*, vol. 86, no. 11, p. 6451-6461, 1999.

[36] N. Ito, Y. Sato, P. K. Song, A. Kaijio, K. Inoue, and Y. Shigesato, “Electrical and optical properties of amorphous indium zinc oxide films,” *Thin Solid Films*, vol. 496, no. 1, pp. 99–103, Feb. 2006.

[37] D. Ginley, H. Hosono, and C. D. Paine, *Handbook of Transparent Conductors*, Ilustrated. 2010.

[38] A. Uygun, O. Turkoglu, S. Sen, E. Ersoy, A. G. Yavuz, and G. G. Batir, “The electrical conductivity properties of polythiophene/TiO2 nanocomposites prepared in the presence of surfactants,” *Curr. Appl. Phys.*, vol. 9, no. 4, pp. 866–871, 2009.

[39] B. Friedel, P. E. Keivanidis, T. J. K. Brenner, A. Abrusci, C. R. McNeill, R. H. Friend, and N. C. Greenham, “Effects of Layer Thickness and Annealing of PEDOT:PSS Layers in Organic Photodetectors,” *Macromolecules*, vol. 42, no. 17, pp. 6741–6747, Sep. 2009.

[40] F. Zhi-Hui, H. Yan-Bing, S. Quan-Min, Q. Li-Fang, L. Yan, Z. Lei, L. Xiao-Jun, T. Feng, W. Yong-Sheng, and X. Rui-Dong, “Polymer solar cells based on a PEDOT:PSS layer spin-coated under the action of an electric field,” *Chinese Phys. B*, vol. 19, no. 3, pp. 1–5, Mar. 2010.

[41] Heraues, “Organic and 3rd generation Solar Cells,” 2015. [Online]. Available: http://www.heraeus-clevios.com/en/applications/solarcells/organic-solar-cells.aspx. [Accessed: 18-Jun-2015].

[42] C. Girotto, E. Voroshazi, D. Cheyns, P. Heremans, and B. P. Rand, “Solution-Processed MoO 3 Thin Films As a Hole-Injection Layer for Organic Solar Cells,” *ACS Appl. Mater. Interfaces*, vol. 3, no. 9, pp. 3244–3247, Sep. 2011.

[43] S. Calnan, “Applications of Oxide Coatings in Photovoltaic Devices,” *Coatings*, vol. 4, no. 1, pp. 162–202, Mar. 2014.

[44] F. Jin, B. Chu, W. Li, Z. Su, B. Zhao, X. Yan, F. Zhang, D. Fan, T. Zhang, Y. Gao, C. S. Lee, and J. Wang, “Improvement in power conversion efficiency and long-term lifetime of organic photovoltaic cells by using bathophenanthroline/molybdenum oxide as compound cathode buffer layer,” *Sol. Energy Mater. Sol. Cells*, vol. 117, pp. 189–193, Oct. 2013.

[45] F. E. Bailey and J. V. Koleske, “Introduction,” in *Poly (ethylene Oxide)*, Elsevier, pp. 1–4, 1976.

[46] F. E. Bailey and J. V. Koleske, “Solution Properties of Poly(ethylene oxide),” in *Poly (ethylene Oxide)*, Elsevier, pp. 29–86, 1976.

[47] C.-S. Liao and W. B. Ye, “Structure and conductive properties of poly(ethylene oxide)/layered double hydroxide nanocomposite polymer electrolytes,” *Electrochim. Acta*, vol. 49, no. 27, pp. 4993–4998, Oct. 2004.

[48] Sigma Aldrich, “Poly(ethylene glycol) and Poly(ethylene oxide),” 2015. [Online]. Available: http://www.sigmaaldrich.com/materials-science/material-science-products.html?TablePage=20204110. [Accessed: 24-Sep-2015].

[49] M. Saboormaleki, A. R. Barnes, and W. S. Schlindwein, “Characterization of Polyethylene Oxide (PEO) Based Polymer Electrolytes,” *Electrochem. Soc.*, 2004.

[50] Sigma Aldrich, “Poly(ethylene oxide),” 2016. [Online]. Available: http://www.sigmaaldrich.com/catalog/product/aldrich/181986?lang=pt&region=PT. [Accessed: 28-Apr-2016].

[51] J. Li, S. G. R. Bade, X. Shan, and Z. Yu, “Single-Layer Light-Emitting Diodes Using Organometal Halide Perovskite/Poly(ethylene oxide) Composite Thin Films,” *Adv. Mater.*, vol. 27, no. 35, pp. 5196–5202, Sep. 2015.

[52] P. Gao, M. Grätzel, and M. K. Nazeeruddin, “Organohalide lead perovskites for photovoltaic applications,” *Energy Environ. Sci.*, vol. 7, no. 8, p. 2448, Jun. 2014.

[53] D. Sabba, H. K. Mulmudi, R. R. Prabhakar, T. Krishnamoorthy, T. Baikie, P. P. Boix, S. Mhaisalkar, and N. Mathews, “Impact of Anionic Br – Substitution on Open Circuit Voltage in Lead Free Perovskite (CsSnI 3-x Br x) Solar Cells,” *J. Phys. Chem. C*, vol. 119, no. 4, pp. 1763–1767, Jan. 2015.

[54] I. Chung, B. Lee, J. He, R. P. H. Chang, and M. G. Kanatzidis, “All-solid-state dye-sensitized solar cells with high efficiency,” *Nature*, vol. 485, no. 7399, pp. 486–489, May 2012.

[55] A. Astefanei, O. Núñez, and M. T. Galceran, “Characterisation and determination of fullerenes: A critical review,” *Anal. Chim. Acta*, vol. 882, pp. 1–21, Jul. 2015.

[56] T. Liu and A. Troisi, “What makes fullerene acceptors special as electron acceptors in organic solar cells and how to replace them,” *Adv. Mater.*, vol. 25, no. 7, pp. 1038–1041, 2013.

[57] Z. Chen, T. Heine, H. Jiao, A. Hirsch, W. Thiel, and P. V. R. Schleyer, “Theoretical studies on the smallest fullerene: from monomer to oligomers and solid States.,” *Chemistry*, vol. 10, no. 4, pp. 963–970, 2004.

[58] H. Derouiche, S. Saidi, and A. B. Mohamed, “The Effect of Energy Levels of the Electron Acceptor Materials on Organic Photovoltaic Cells,” *Smart Grid Renew. Energy*, vol. 02, no. 03, pp. 278–281, 2011.

[59] A. I. Podlivaev and L. A. Openov, “Formation of a ‘cluster molecule’ (C20)2 and its thermal stability,” *Phys. Solid State*, vol. 48, no. 11, pp. 2226–2232, Nov. 2006.

[60] G. B. Adams, M. O’Keeffe, and R. S. Ruoff, “Van Der Waals Surface Areas and Volumes of Fullerenes,” *J. Phys. Chem.*, vol. 98, no. 38, pp. 9465–9469, Sep. 1994.

[61] K. Hedberg, L. Hedberg, D. S. Bethune, C. A. Brown, H. C. Dorn, R. D. Johnson, and M. DE Vries, “Bond lengths in free molecules of buckminsterfullerene, c60, from gas-phase electron diffraction.,” *Science*, vol. 254, no. 5030, pp. 410–412, 1991.

[62] M. S. Dresselhaus and G. Dresslhaus, “Fullerenes and Fullerene Derived Solids as Electronic Materials,” *Annu. Rev. Mater. Sci.*, vol. 25, no. 1, pp. 487–523, Aug. 1995.

[63] Y. Li, Y. Huang, S. Du, and R. Liu, “Structures and stabilities of C60-rings,” *Chem. Phys. Lett.*, vol. 335, no. 5–6, pp. 524–532, Mar. 2001.

[64] M. Qian, M. Li, X. B. Shi, H. Ma, Z. K. Wang, and L. S. Liao, “Planar perovskite solar cells with 15.75% power conversion efficiency by cathode and anode interfacial modification,” *J. Mater. Chem. A*, vol. 3, no. 25, pp. 13533–13539, 2015.

[65] Sigma Aldrich, “Bathophenanthroline,” 2015. [Online]. Available: http://www.sigmaaldrich.com/catalog/product/aldrich/133159?lang=pt&region=PT. [Accessed: 26-Sep-2015].

[66] H. L. Cheng and K.-F. Lin, “Enhancing emission of poly(p-phenylenevinylene) by sandwiching an energy transferable layer,” *J. Mater. Chem.*, vol. 12, no. 8, pp. 2270–2274, Jul. 2002.

[67] C. J. Brabec, S. E. Shaheen, C. Winder, N. S. Sariciftci, and P. Denk, “Effect of LiF/metal electrodes on the performance of plastic solar cells,” *Appl. Phys. Lett.*, vol. 80, no. 7, pp. 1288–1290, 2002.

[68] T. Yu, Y. Cao, W. Su, C. Zhang, Y. Zhao, D. Fan, M. Huang, K. Yue, and S. Z. D. Cheng, “Synthesis, structure, photo- and electro-luminescence of an iridium complex with a novel carbazole functionalized β-diketone ligand,” *RSC Adv.*, vol. 4, no. 2, pp. 554–562, 2014.

[69] Y. S. Eo, H. W. Rhee, B. D. Chin, and J.-W. Yu, “Influence of metal cathode for organic photovoltaic device performance,” *Synth. Met.*, vol. 159, pp. 1910–1913, 2009.

[70] G. Del Pozo, B. Romero, and B. Arredondo, “Influence of cathode in organic solar cells performance,” in *Proceedings of the 2013 Spanish Conference on Electron Devices, CDE 2013*, no. 1, pp. 321–324, 2013.

[71] C. N. Carvalho, A. Luis, G. Lavareda, E. Fortunato, and A. Amaral, “Effect of thickness on the properties of ITO thin films deposited by RF-PERTE on unheated, flexible, transparent substrates,” *Surf. Coatings Technol.*, vol. 151–152, pp. 252–256, Mar. 2002.

[72] K. Sugiyama, H. Ishii, Y. Ouchi, and K. Seki, “Dependence of indium–tin–oxide work function on surface cleaning method as studied by ultraviolet and x-ray photoemission spectroscopies,” *J. Appl. Phys.*, vol. 87, no. 1, p. 295, 2000.

[73] K. B. Lim and D. C. Lee, “Surface modification of glass and glass fibres by plasma surface treatment,” *Surf. Interface Anal.*, vol. 36, no. 3, pp. 254–258, 2004.

[74] S. H. Tan, N. T. Nguyen, Y. C. Chua, and T. G. Kang, “Oxygen plasma treatment for reducing hydrophobicity of a sealed polydimethylsiloxane microchannel,” *Biomicrofluidics*, vol. 4, no. 3, 2010.

[75] C. P. Division, “Clevios™ P VP Ai 4083,” *CLEVIOS P VP AI 4083*, pp. 1–2, 2010.

[76] A. Berni, M. Menning, and H. Schmidt, “Sol-Gel Technologies for Glass Producers and Users - Doctor Blade,” in *Sol-Gel Technologies for Glass Producers and Users*, M. A. Aegerter and M. Mennig, Eds. Boston, MA: Springer US, pp. 37 – 48, 2004.

[77] A. Dualeh, N. Tétreault, T. Moehl, P. Gao, M. K. Nazeeruddin, and M. Grätzel, “Effect of Annealing Temperature on Film Morphology of Organic-Inorganic Hybrid Pervoskite Solid-State Solar Cells,” *Adv. Funct. Mater.*, vol. 24, no. 21, pp. 3250–3258, Jun. 2014.

[78] J. Farinhas, Q. Ferreira, R. E. Di Paolo, L. Alcácer, J. Morgado, and A. Charas, “Nanostructured donor/acceptor interfaces in photovoltaic cells using columnar-grain films of a cross-linked poly(fluorene-alt-bithiophene),” *J. Mater. Chem.*, vol. 21, no. 33, pp. 12511–12519, 2011.

[79] K. Reichelt and X. Jiang, “The preparation of thin films by physical vapour deposition methods,” *Thin Solid Films*, vol. 191, no. 1, pp. 91–126, Oct. 1990.

[80] Sigma Aldrich, “Product Specification - Fullerene C60 - 99.5%.” Sigma Aldrich, Saint Loius, USA, pp. 1–2, 2015.

[81] Sigma Aldrich, “[6,6]-phenyl-C61-butyric acid methyl ester.” Sigma Aldrich, Saint Loius, USA, p. 1, 2015.

[82] Oriel Instruments, “Oriel Sol3A ™ Class AAA Solar Simulators,” 2007.

[83] University of Washington, “Physics of Solar Cells.” [Online]. Available: http://depts.washington.edu/cmditr/modules/opv/physics_of_solar_cells.html. [Accessed: 07-Jan-2015].

[84] P. Stallinga, *Electrical Characterization of Organic Electronic Materials and Devices*. Chichester, UK: John Wiley & Sons, Ltd, 2009.

[85] D. Liu, M. K. Gangishetty, and T. L. Kelly, “Effect of CH 3 NH 3 PbI 3 thickness on device efficiency in planar heterojunction perovskite solar cells,” *J. Mater. Chem. A*, vol. 2, no. 46, pp. 19873–19881, Oct. 2014.

[86] H. K. Hughes and H. K. Hughes, “Beer’s Law and the Optimum Transmittance in Absorption Measurements,” *Appl. Opt.*, vol. 2, no. 9, pp. 937–945, 1963.

[87] J. M. Parnis and K. B. Oldham, “Beyond the Beer–Lambert law: The dependence of absorbance on time in photochemistry,” *J. Photochem. Photobiol. A Chem.*, vol. 267, pp. 6–10, Sep. 2013.

[88] H. S. Ko, J. W. Lee, and N. G. Park, “15.76% efficiency perovskite solar cells prepared under high relative humidity: importance of PbI 2 morphology in two-step deposition of CH 3 NH 3 PbI 3,” *J. Mater. Chem. A*, vol. 3, no. 16, pp. 8808–8815, 2015.

[89] J. Burschka, N. Pellet, S. J. Moon, R. Humphry-Baker, P. Gao, M. K. Nazeeruddin, and M. Grätzel, “Sequential deposition as a route to high-performance perovskite-sensitized solar cells,” *Nature*, vol. 499, no. 7458, pp. 316–319, Jul. 2013.

[90] M. Grätzel, “EPFL Achieves 21% Efficiency for Perovskites,” DYESOL LTD, p. 1, Dec. 2015.